

CHEMICAL PROGRAMMING OF MACROPHAGES VIA DIRECT  
ACTIVATING RECEPTOR LABELING FOR TARGETED  
TUMOUR IMMUNOTHERAPY

# CHEMICAL PROGRAMMING OF MACROPHAGES VIA DIRECT ACTIVATING RECEPTOR LABELING FOR TARGETED TUMOUR IMMUNOTHERAPY

Zi Ling (Sissi) Yang and Anthony F. Rullo

Department of Chemistry and Chemical Biology & Department of Medicine  
McMaster University

September 6<sup>th</sup>, 2023

McMaster University

© Copyright by Zi Ling Yang

McMaster University MASTER OF SCIENCE (2023) Hamilton, Ontario (Science)

TITLE: Chemical Programming of Macrophages for via Direct Activating Receptor Labeling for Targeted Tumour Immunotherapy

AUTHOR: Zi Ling Yang, B.Sc. (McMaster University)

SUPERVISOR: Professor Anthony F. Rullo

NUMBER OF PAGES: 87

## Abstract

Antibody-recruiting molecules (ARMs) are therapeutic tools that simultaneously bind a hapten-specific serum antibody and a cancer cell surface protein, resulting in the activation and recruitment of an immune cell to the cancer surface. However, ARM efficacy is limited by the ability of ARMs to form a quaternary complex with the immune cell receptor, antibody, and cancer cell surface. The Rullo lab has previously developed and characterized a covalent ARM (cARM) that irreversibly links the ARM to the antibody and simplifies the quaternary binding equilibria. cARMs have shown a marked increase in both target immune recognition and therapeutic efficacy. However, cARM efficacy is still limited by the affinity of the antibody for the immune receptor. We aim to investigate how direct covalent engagement of the immune receptor and elimination the antibody-immune receptor binding equilibria impacts immune activation and therapeutic efficacy.

This thesis focuses on the chemical programming of macrophages through direct covalent immune receptor engagement. We have developed and characterized covalent immune programmers (CIPs), which are molecules that contain a macrophage targeting domain and a tumour targeting domain. The macrophage targeting domain binds the activating receptor CD64 on the macrophage surface and contains a chemical warhead that covalently labels the receptor once bound. The tumour targeting domain can promote macrophage tumour engagement resulting in tumoricidal function. Flow cytometry experiments have shown that CIPS are able to bind Fc receptors specifically and effectively on the surface of macrophages. Further, CIPs were able to induce macrophage activation and induce target specific phagocytosis. These experiments have also shown that direct engagement of the receptor by the CIP is more effective than antibody-mediated engagement, suggesting that overall immune complex stability affects immune cell activation. Taken together, these concepts can be used to guide future immunotherapeutic design.

## Acknowledgements

Thank you to Dr. Anthony Rullo for your guidance and mentorship throughout my graduate studies. I am grateful for the opportunity to work in your laboratory and for everything that I have learned because of my time here.

Thank you to all the members of the Rullo Lab I have worked with, both past and present: Eden Kapcan, Karolina Krygier, Arthur Srayeddin, Sandra Hwang, Rebecca Turner, Sarah Eisinga, Akshaya Raajkumar, Benjamin Lake, Harrison McCaan, Maya Da Luz, Tomas Frankovich, Mauro Castellarin, and Nick Serniuck. A special thanks to Eden Kapcan, Rebecca Turner, and Mauro Castellarin for your help on this project.

Thank you to my committee members Dr. Katherine Bujold and Dr. Shelia Singh for your input and guidance throughout this project.

Table of Contents

<b>1. Introduction</b>	<b>1</b>
1.1 Immunotherapeutic Design and Development	1
1.1.1 The Importance of Cancer Treatment Innovation	1
1.1.2 Immunotherapy: Advantages and Limitations	1
	3
1.2 Macrophages as a Target for Cancer Immunotherapy Design	
1.2.1 Placing Macrophages in Context of the Overall Immune System	3
1.2.2 Unique Characteristics of Macrophages Make it A Good Target for Immunotherapeutic Design	5
1.2.3 Types of Macrophages and Tumor Associated Macrophages	6
	7
1.3 Current Immunotherapeutic Strategies Targeting Macrophages	
1.3.1 Re-programming TAMs	7
1.3.2 Metabolic Glycoengineering	9
1.3.3 Chimeric Antigen Receptor Macrophages	11
1.3.4 Monoclonal Antibodies and Antibody Recruiting Molecules	12
1.4 Designing Covalent Immune Programmable (CIPs)	15
1.4.1 CIPs: Direct Activating Receptor Labeling Improves on Previous Technologies	15
1.4.2 Sulfonyl Fluoride Exchange Chemistry (SuFEx)	19
1.4.3 Tumour Targeting Domains	20
1.5 Project Objectives	21
<b>2. Materials and Methods</b>	<b>22</b>
2.1 Synthetic Methods	22
2.1.1 Solid phase peptide synthesis general procedures	22
2.1.2 Covalent cP33 synthesis	23
2.1.3 AE133-DBCO synthesis	23
2.1.4 Installation of reporter molecules or the tumor targeting domain	24

Table of Contents

2.2 Fluorescent SDS-PAGE	25
2.2.1 General fluorescent SDS-PAGE procedures	25
2.2.2 CIP specificity SDS-PAGE assay	25
2.2.3 CIP kinetics SDS-PAGE assay	26
2.3 MALDI	26
2.4 Aqueous Stability Studies	27
2.5 Bio-layer Interferometry Binding Assays	27
2.6 Cell Surface CD64 Labeling Flow Cytometry Assay	28
2.6.1 General Protocol	28
2.6.2 Installation of the Biotin Domain Post Cell Surface CD64 Labeling via SPAAC	29
2.7 Two-colour Phagocytosis Assay	30
2.7.1 General Protocol	30
2.7.2 CIP-biotin streptavidin bead phagocytosis assay	31
2.7.3 CIP-AE133 uPAR bead phagocytosis assay	32
2.8 THP1 NF-kB Activation Reporter Cell Assay	32
	33
<b>3. Results and Discussion</b>	
3.1 CIP Design	<b>33</b>
3.2 CIP Synthesis	34
3.3 CIP can Selectively and Covalently Label CD64 in Solution	40
3.4 CIP can Specifically and Covalently Label CD64 on the Immune Cell Surface	42
3.5 Optimizing Covalent Electrophile Position	45
3.6 Tumor Targeting Domains can be Installed on the Immune Cell Surface via CIPs	50
3.7 CIPs can Promote Immune Activation	52
3.8 Future Directions: CIP-AE133 can be used to Target uPAR	58
	61
<b>4. Conclusions and Future Directions</b>	
4.1 Conclusions	<b>61</b>
4.2 Future Directions	62
	<b>64</b>
<b>5. References</b>	
	<b>70</b>
<b>6. Appendix</b>	

## List of Figures

Figure 1. Surface functionalized of macrophages with Tumour Binding Aptamers via Metabolic Glycoengineering	11
Figure 2. CAR-Macrophage Function.	12
Figure 3. Schematic Illustrating Antibody Recruiting Molecule Function.	14
Figure 4. Covalent Antibody Recruiting Molecules Simplify Complex Formation.	15
Figure 5. Molecular modelling of cP33 peptide complexed to CD64.	17
Figure 6. Structure of cP33 peptide.	17
Figure 7. Schematic illustrating covalent immune programmer function.	18
Figure 8. SuFEx reaction mechanism.	19
Figure 9. Modified AE133 Peptide Structure.	21
Figure 10. Aspartimide formation.	35
Figure 11. Chemical structure of CIP analogs.	37
Figure 12. CIP Synthetic Scheme.	38
Figure 13. Chemical Structure of CIP Targeting Analogs	39
Figure 14. Nt-CIP <i>in solution</i> CD64 labeling specificity	41
Figure 15. Nt-CIP CD64 Labeling MALDI Spectra	42
Figure 16. CIP monocyte cell surface CD64 labeling	44
Figure 17. CIP electrophile analog kinetics.	46
Figure 18. CIP aqueous stability studies showing the UV trace from LC-MS analysis.	48
Figure 19. Covalent electrophile position affects cell surface CD64 labeling.	50
Figure 20. Installation of the targeting domain on the cell surface using SPAAC click chemistry.	51
Figure 21. THP1 NF- $\kappa$ B-Luc2 Macrophage Luciferase Activation Assay.	53
Figure 22. Evaluation of CIP ability to induce targeted phagocytosis.	55
Figure 23. Comparing the ability of CIPs and an antibody-based treatment (cARM) to induce phagocytosis using a two-colour flow cytometry assay.	58
Figure 24. Characterizing CIP-AE133 ternary complex formation using BLI.	59

## List of Figures

Figure 25. Evaluating CIP-AE133 ability to induce phagocytosis of uPAR labeled targets.	61
Appendix 1. LC-MS of purified Nt-CIP-Az.	70
Appendix 2. LC-MS of purified Int-CIP-Az.	71
Appendix 3. LC-MS of purified Ct-CIP-Az.	72
Appendix 4. Determination of IEDDA click strategy labeling efficacy.	73
Appendix 5. LC-MS of CIP-AE133.	74

## List of Tables

Table 1. Ligands that can reprogram immunosuppressive macrophages through activating receptors.	8
Table 2. CIP electrophile analog $k_{\text{obs}}$ labeling rate constants.	47

Abbreviations

<b>ACN</b>	Acetonitrile
<b>ADCC</b>	Antibody-dependent cellular cytotoxicity
<b>ADCP</b>	Antibody-dependent cellular phagocytosis
<b>ARM</b>	Antibody recruiting molecule
<b>BLI</b>	Bio-layer interferometry
<b>CAR</b>	Chimeric antigen receptor
<b>cARM</b>	Covalent antibody recruiting molecule
<b>CD64</b>	Cluster of Differentiation 64
<b>CIP</b>	Covalent immune programmer
<b>DBCO</b>	Dibenzocyclooctyne
<b>DCM</b>	Dichloromethane
<b>DDE</b>	N -[1-(4,4-dimethyl-2,6-dioxocyclohex-1-ylidene)ethyl]
<b>DIC</b>	N,N'-Diisopropylcarbodiimide
<b>DIPEA</b>	N,N-Diisopropylethylamine
<b>Dmb</b>	2,4-Dimethoxybenzyl
<b>DMEM</b>	Dulbecco's Modified Eagle's Medium
<b>DMF</b>	Dimethyl formamide
<b>DMSO</b>	Dimethylsulfoxide
<b>DNP</b>	2,4-Dinitrophenol
<b>ECM</b>	Extracellular matrix
<b>FBS</b>	Fetal bovine serum
<b>Fmoc</b>	Fluorenylmethoxycarbonyl
<b>HPLC</b>	High-performance liquid chromatography
<b>IEDDA</b>	Inverse electron demand Diels-Alder
<b>IFN<math>\gamma</math></b>	Interferon gamma
<b>LCMS</b>	Liquid chromatography-mass spectrometry
<b>MALDI</b>	Matrix-assisted laser desorption/ionization
<b>Mmt</b>	Monomethoxytrityl
<b>nCIP</b>	Non-covalent immune programmer

<b>NCS</b>	N-Chlorosuccinimide
<b>NHS</b>	N-Hydroxysuccinimide
<b>PBS</b>	Phosphate buffered saline
<b>PE</b>	Phycoerythrin
<b>PEG</b>	Polyethylene glycol
<b>PSMA</b>	Prostate specific membrane antigen
<b>RPMI</b>	Roswell Park Memorial Institute 1640 Medium
<b>SDS-PAGE</b>	Sodium dodecyl-sulfate polyacrylamide gel electrophoresis
<b>SPAAC</b>	Strain-promoted azide-alkyne cycloaddition
<b>SPPS</b>	Solid-phase peptide synthesis
<b>SuFEx</b>	Sulfonyl fluoride exchange
<b>TAM</b>	Tumour associated macrophage
<b>TCO</b>	Trans cyclo-octyne
<b>TFA</b>	Trifluoroacetic acid
<b>TIPS</b>	Triisopropyl silane
<b>uPA</b>	Urokinase plasminogen activator
<b>uPAR</b>	Urokinase plasminogen activator receptor

## Declaration of Academic Achievement

Towards the completion of this thesis, Zi Ling Yang was responsible for the synthesis of characterization of each final construct. Some synthesis optimization was completed with the help of Rebecca Turner and Eden Kapcan. Additionally, Zi was responsible for all kinetics labeling and selectivity studies as well as all flow cytometry studies (including cell labeling and phagocytosis assays). Lastly, Zi completed each illustration and assembled all results towards the completion of this report.

All THP1-NF-kB immune cell activation assays were performed by Dr. Mauro Castellarin.

All MALDI experiments was done by Dr. Yang Yang from the McMaster Biointerfaces Institute Core.

## 1. Introduction

### 1.1 Immunotherapeutic Design and Development

#### **1.1.1 The Importance of Cancer Treatment Innovation**

Cancer is responsible for one in six deaths and is considered one of the leading causes of death globally.<sup>1</sup> There were 19.3 million new cancer cases and 10 million deaths from cancer worldwide in 2020. Global trends project that these numbers will only continue to rise and result in an ever-increasing burden on healthcare systems.<sup>2</sup> Traditionally, cancer is treated with surgical removal of the tumor followed by radiotherapy or chemotherapy.<sup>3</sup> However, cancer treatment is a very complex process and current conventional methods of treatment suffer from many limitations.<sup>4</sup> Notably, chemotherapy and radiation therapy will damage healthy cells, leading to harmful side effects. The heterogeneity and rapid growth of the cancer cell population frequently result in them developing resistance to previously effective anti-cancer drugs via selective pressure.<sup>5</sup> Taken together, the increasing cancer incidence rates and limitation of current treatment options illustrates the need for the development of novel cancer treatment strategies.

#### **1.1.2 Immunotherapy: Advantages and Limitations**

Immunotherapy has quickly established itself as one of the most promising innovations in cancer treatment. It works by harnessing the body's endogenous immune system to target and destroy cancerous cells.<sup>6</sup> There are many different methods of immunotherapeutic treatment. Some of the most popular currently approved for clinical use include adoptive cell therapy, immunomodulators, and monoclonal antibodies. Adoptive cell therapy involves administering activated immune cells that have been engineered to recognize a cancer specific antigen and therefore target and attack

cancerous cells.<sup>6,7</sup> Immunomodulators are drugs that can manipulate the pro-inflammatory or anti-inflammatory signals that regulate the immune system.<sup>8</sup> Cytokines such as IL-2 are known to promote activation and growth of immune cells and although are approved as a monotherapy in high doses, are often used in combination with other treatments.<sup>9,10</sup> Another type of immunomodulator are immune checkpoint inhibitors, such as PD-1 or PD-L1 inhibitors.<sup>11-13</sup> Immune checkpoint inhibitory ligands bind to immune checkpoint receptors on the surface of an immune cell and limit immune cell activity to prevent autoimmune disease. The over-expression of immune checkpoint inhibitor ligands on cancer cells leads to cancer immune resistance. To re-establish anti-tumour immunity, these immune checkpoint inhibitor ligands can be inhibited by immune checkpoint inhibitors. Monoclonal antibodies work by binding a tumour specific antigen and recruiting immune cells to the site of the tumour to promote an immune response.<sup>14,15</sup>

Because of the immune system's intrinsic ability to recognize targets with high specificity, immunotherapeutics are often highly specific and result in less damage to healthy cells compared to traditional treatments, leading to less toxic side effects.<sup>16-18</sup> Immunotherapeutic treatments also often have high remission rates and show an enhancement in progression-free survival and overall survival. Unlike conventional methods of treatment, immunotherapies are also more dynamic and have been shown to persist long-term within the patient, allowing for better long-term survival and antitumoral immunity.<sup>19,20</sup>

Despite these promising advantages, cancer immune evasion presents a limitation on immunotherapeutic efficacy.<sup>21,22</sup> Immune cells target and destroy

cancerous cell via recognition of specific cancer antigens. However, this can apply a selective pressure for cancer cell variants that have low levels of immunogenic antigen expression and escape immune surveillance. These less immunogenic cancer cells can grow and proliferate, allowing the cancer to evolve mechanisms of immune evasion. Further, the tumour microenvironment can also have a great effect on immunotherapeutic efficacy. Tumours can be described as immunologically hot or immunologically cold.<sup>23-25</sup> Immunologically hot tumours are associated with high levels of pro-inflammatory cytokines, increased T-cell infiltration and high mutational load leading to the accumulation of immunogenic neoantigens. These characteristics lend themselves to more successful immunotherapeutic treatment and clinical outcomes. In contrast, the characteristics of immunologically cold tumours counteract the mechanisms through which immunotherapies work and results in poor clinical outcomes. Cold tumours have decreased lymphocyte infiltration and a lower mutational load resulting in fewer neoantigens that can be targeted. Further, often present in the tumour microenvironment of cold tumours are immune cells that secrete immunosuppressive signals and promote tumour growth.

## 1.2 Macrophages as a Target for Cancer Immunotherapy Design

### 1.2.1 Placing Macrophages in Context of the Overall Immune System

The immune system is a very complex network of immune cells and biochemical signals that synergize to discriminate foreign pathogens from host cells. There are two parts of the immune system: the innate and adaptive immune system.<sup>26</sup> Broadly, the innate system recognizes very general molecular patterns on a broad range of microbes and toxins that are not present on host cells. It can not be modified by or retain memory

of previous responses. The innate immune system includes bioactive proteins and small molecules that are constitutively expressed (e.g. complement proteins) or are released from activated immune cells (e.g. cytokines, reactive free radicals, chemokines). It also includes circulating immune cells such as monocytes and macrophages.<sup>27</sup> These cells contain surface receptors that bind antigens expressed on the surface of foreign pathogens and initiate an immune response which kills the pathogen through mechanisms such as phagocytosis or free radical formation.<sup>26-28</sup> This system forms a very rapid response and is thus considered the “first response” of the immune system.

If the innate immune system cannot clear the pathogen, the adaptive immune system is recruited to compose a very highly specific immune response to a particular foreign antigen.<sup>26-28</sup> This system adapts its immunity based on previous responses and is therefore responsible for long-term responses to pathogens. The adaptive immune system is mostly composed of B-cells and T-cells. B-cells are responsible for producing antibodies that can activate and direct immune recognition. B-cells are also antigen presenting cells that can present processed antigen to activate T-cells. T-cells have receptors that directly recognize the antigen. There are two types of T cells: cytotoxic T-cells that destroy pathogens and helper T-cells that direct other immune cells to promote an immune response.<sup>29</sup> While macrophages have been discussed in the context of the innate immune system, they also play a role in the adaptive immune system.<sup>27</sup> In this system, they can also act as antigen presenting cells that present their phagocytosed antigens to T cells.

### **1.2.2 Unique Characteristics of Macrophages Make it A Good Target for Immunotherapeutic Design**

Previous studies have reported that cancer development is low in invertebrates with no T-cells or B-cells (parts of the adaptive immune system), which suggests that the innate immune system is important in preventing initial cancer formation and proliferation.<sup>30,31</sup> Their wide range of roles in the immune system, as well as how they function both within the innate and adaptive immune system, make macrophages a good innate immune cell to target as an effector in immunotherapeutic design. They can directly destroy target cells through processes such as phagocytosis and reactive oxygen species generation.<sup>32</sup> Due to their role as activators and regulators, macrophages activated against tumour antigens can also activate and direct other immune cells to promote a wide immune response. They can secrete pro-inflammatory cytokines and recruit other immune cells to the site of inflammation. Further, as antigen presenting cells, they can promote an adaptive immune response, resulting in not only an immediate therapeutic effect but also long-term anti-cancer immunity.<sup>27</sup>

Macrophages also have many unique characteristics that make it a promising target for immunotherapeutic effector development. Entry into solid tumours is difficult for T-cells and therefore T-cell based therapies are limited by low infiltration.<sup>32</sup> However, macrophages can easily infiltrate into tumours and represent 30-50% of the total immune cell population in the tumour microenvironment. To illustrate the ability of macrophages to infiltrate tumours, a study showed that macrophages loaded with a drug-containing nanoparticle were able to reach the tumour site more efficiently than the free nanoparticle.<sup>33</sup> Macrophages are also easily accessible, allowing for facile collection, modification, and drug binding in a clinical setting.<sup>32</sup> This is because

monocytes are a major source of tumour infiltrating macrophages and they are one of the most abundant white blood cells, making up 5-12% of the population of leukocytes circulating in the blood. Further, the idea of tumour immune escape via clearance of high antigen expressing cancer cells has been introduced previously in this review. As an innate immune cell, macrophages can still be activated for anti-tumoricidal activity without the need to target one specific antigen, in contrast with adaptive immune cells.<sup>34,35</sup> Targeting a single specific antigen is difficult in cases where the specific antigen is still expressed on non-cancerous cells or tumour heterogeneity results in cancer cells expressing multiple antigens.<sup>32</sup>

### **1.2.3 Types of Macrophages and Tumor Associated Macrophages**

Although macrophages have been previously characterized in a binary M1 (pro-inflammatory) and M2 (anti-inflammatory) system, it's now understood that macrophages exist on a wide spectrum of phenotypes depending on developmental origin, tissues of residence, and microenvironmental conditions (including signalling proteins).<sup>36-40</sup> This wide phenotypic spectrum is reflected in the functional plasticity of macrophages. They have a role in regulating angiogenesis, tissue remodelling, pro-inflammatory immune responses and immunosuppression, among many others.

The tumour microenvironment has a combination of elements (including fibrosis, hypoxia, nutrient availability, and lymphocyte-derived factors) that results in the recruitment and promotion of tumour associated macrophages (TAMs).<sup>41</sup> TAMs promote tumour angiogenesis, which allows tumours access to the oxygen and nutrients needed for growth, by expressing factors such as WNT7B, VEGF-C, VEGF-D and many others.<sup>42-45</sup> They also enhance tumour hypoxia and glycolysis which are causes of

angiogenesis.<sup>46-48</sup> TAMs also promote cancer metastasis by dissolving the extracellular matrix through the expression of matrix metalloproteinases, cathepsin, urokinase plasminogen activator, and matrix remodelling enzymes.<sup>49</sup> This allows for tumour cell escape. Secretion of cytokines and growth factors by TAMs also promotes cancer cell invasiveness.<sup>50,32</sup> In this way, TAMs have a negative effect on patient survival.

In addition, TAMs display an immune-suppressive phenotype. TAMs establish an immune-suppressive tumour microenvironment through three main methods: 1) consuming metabolites needed for T-cell activation, 2) secreting inhibitory cytokines that prevent immune cell function and activation, and 3) expressing inhibitory receptors via antigen presentation.<sup>51</sup> As such, they reduce the efficacy of immunotherapies and hinder the ability of the natural immune system to target the tumour. The ability to target these TAMs and re-program them from a tumour-promoting state to a pro-inflammatory state would be greatly advantageous for treatment.

## 1.3 Current Immunotherapeutic Strategies Targeting Macrophages

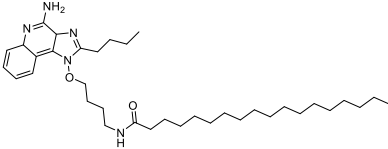
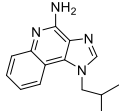
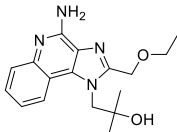
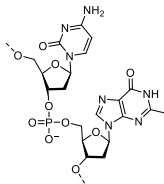
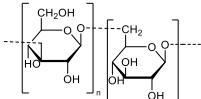
### 1.3.1 Re-programming TAMs

Due to their significant impact on clinical outcome, TAMs have established themselves as a promising target for cancer immunotherapy. The functional plasticity of macrophages allows for the possibility of re-programming TAMs to inhibit pro-tumour activity and display an anti-tumour/pro-inflammatory phenotype.<sup>52</sup> There have been many methods of TAM re-programming that have been studied in literature.

Most notably, activation of Toll-like receptors (TLRs) on the macrophage surface have been shown to promote a pro-inflammatory phenotype. Studies have shown that delivery of a TLR7/8 agonist known as 3M-052 re-programmed TAMs to a reactive

oxygen species producing pro-inflammatory phenotype.<sup>53</sup> This improved the anti-tumour immune response and resulted in elimination of murine metastatic melanoma. Further, combining 3M-052 with immune checkpoint inhibitors targeting CTLA-4 and PD-L1 can synergistically rescue TAM and T-cell anti-tumoral activity. Imiquimod, a TLR7 agonist, is currently approved for clinical use and has shown efficacy in combination therapies against basal cell carcinoma, melanoma, and cutaneous metastases of breast cancer.<sup>54</sup>

CD40 is another key activating receptor that can reprogram TAMs. CD40 activation with monoclonal antibodies was shown to promote anti-tumoral activity and pro-inflammatory cytokine production.<sup>55</sup> Table 1 shows an overview of select ligands that can re-program immunosuppressive macrophages for further consideration.

Ligand	Receptor Targeted	Structure
3M-052 <sup>53</sup>	TLR7/8	
Imiquimod <sup>54</sup>	TLR7	
Resiquimod <sup>56</sup>	TLR7/8	
Cytosine guanine oligodeoxynucleotide (CpG motif) <sup>57</sup>	TLR9	
IFN $\gamma$ <sup>58</sup> Sotigalimab, <sup>55,59</sup> B-Glucan <sup>60</sup>	Interferon- $\gamma$ receptor CD40 Dectin-1	Cytokine, two domain homodimer Monoclonal antibody 

**Table 1.** Ligands that can reprogram immunosuppressive macrophages through activating receptors.

Inhibition of several different signalling pathways in TAMs have been shown to successfully re-program macrophages. Suppression of the PI3K $\gamma$  signaling pathway has re-instated pro-inflammatory activity in TAMs and slowed tumour growth.<sup>61</sup> Similarly, inhibition of hedgehog signalling in TAMs increased pro-inflammatory cytokine production while suppressing anti-inflammatory activity in mouse hepatoma and Lewis lung carcinoma.<sup>62</sup>

Another method of TAM re-programming is mRNA based. A study used nanoparticles containing two mRNA sequences that encode for pro-inflammatory signals into TAM cells.<sup>63</sup> The first sequence codes for IRF5, an interferon regulatory factor family, and the second sequence codes for IKK $\beta$ , a kinase that phosphorylates and activates IRF5. Together, they were able to downregulate expression of genes encoding immuno-suppressive activity and upregulate the pro-inflammatory CCL5 gene. This mRNA treatment was able to re-program TAMs to display pro-inflammatory activity and increased T-cell tumour infiltration in a murine ovarian tumour model. Ex-vivo treated TAMs showed an increase in pro-inflammatory cytokine secretion levels.

### **1.3.2 Metabolic Glycoengineering**

Metabolic glycoengineering describes the process of incorporating unnatural sugars into the glycans on the cell surface.<sup>64</sup> This is done by growing these cells in the presence of the target unnatural monosaccharides and allowing the cells to uptake and incorporate the sugar during biosynthesis. These unnatural monosaccharides can include functional group side chains, allowing the surface of the cell to be labelled with functional groups that can be further chemically modified. Previous uses of metabolic

glycoengineering in cancer treatment include the metabolic glycoengineering of tumour cells with azide-modified tetraacetyl-*N*-azidoacetylmannosamine sugars.<sup>65</sup> This functionalized the tumour cell surface with azide click handles. The azides on the cell surface can bio-orthogonally react with DBCO molecules via strain-promoted alkyne-azide click chemistry, serving as a method to chemically introduce a highly specific binding antigen or receptor. In this study, the researchers were able to specifically label the cancer cell surface with a DBCO-labelled chemotherapeutic drug, reducing the off-target effect of the chemotherapeutic and effectively improving survival rate compared to the free drug.

Metabolic glycoengineering has also been used to functionalize macrophage cells for tumour immunotherapy. A study used this method to attach nucleic acid aptamers that bind tumour membrane proteins (Figure 3) to the immune cell surface.<sup>66</sup> The study showed that the glycoengineered macrophages resulted in an increase in tumour adherence and engagement. When the tumours were treated with an apoptosis inducing agent, the aptamer-labelled macrophages were shown to effectively phagocytose the tumour cells. After phagocytosis, the major histocompatibility complex (required for antigen presentation) expression levels increased. Notably, the metabolically glycoengineered macrophages were unable to phagocytose the tumour cells that were not apoptosed. This is likely the result of the lack of activating signal present to stimulate macrophage activity and illustrates that adherence alone is not sufficient for effective macrophage activation for immunotherapy.

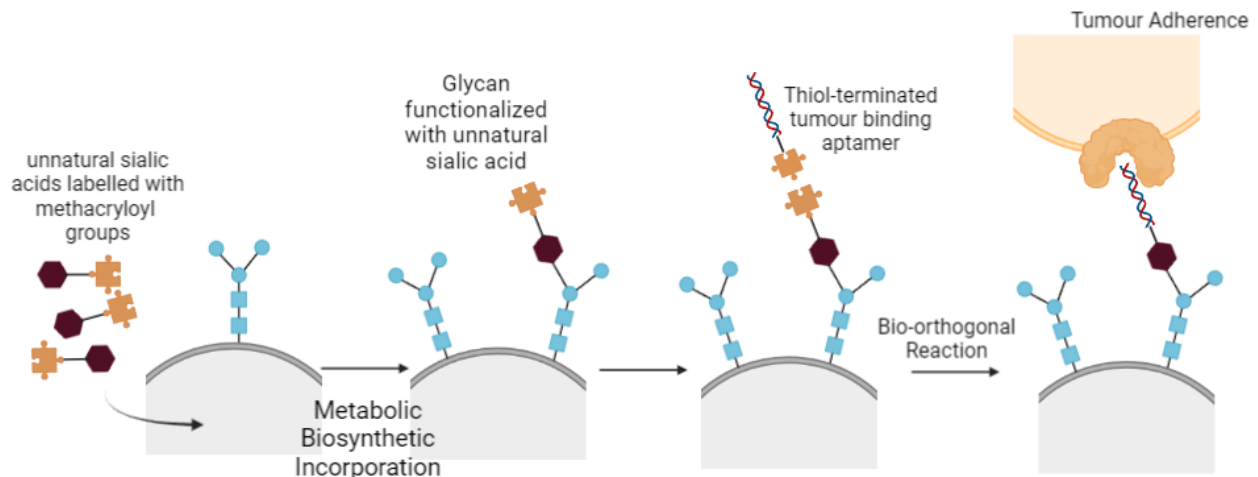


**Figure 1. Surface functionalized of macrophages with Tumour Binding Aptamers via Metabolic Glycoengineering.** Unnatural sialic acids (red) labelled with methacryloyl groups (yellow) are incorporated into glycans on the cell surface via biosynthesis. The thiol group on the end of the tumour binding aptamer can react with the methacryloyl groups on the macrophage cell surface. Macrophages labelled with the aptamer can engage and adhere to tumour cells. Figure created in Biorender.

### 1.3.3 Chimeric Antigen Receptor Macrophages

CAR-T cell therapy is a type of adoptive cell transfer therapy that involves genetically engineering the patients' endogenous T-cells to express a chimeric antigen receptor (CAR) that binds a specific tumour antigen.<sup>67</sup> Upon binding, the receptor activates the T-cell to promote an anti-tumoral immune response. CAR-T cell therapy has shown great promise in the clinic; however, they still have limited efficacy for solid tumours.

Studies have reported the successful synthesis of CAR-macrophages that express CAR receptors on the cell surface.<sup>68</sup> CAR-macrophages have demonstrated antigen specific phagocytosis *in vivo* and prolonged overall survival *in vivo*. These

macrophages showed a sustained pro-inflammatory phenotype and express pro-inflammatory cytokines and chemokines. Notably, CAR-macrophages have also been able to convert nearby anti-inflammatory macrophages into pro-inflammatory macrophages. They were also able to activate T-cells via antigen presentation. However, CAR cell therapy can be less accessible due to specialized and long manufacturing process and high costs.

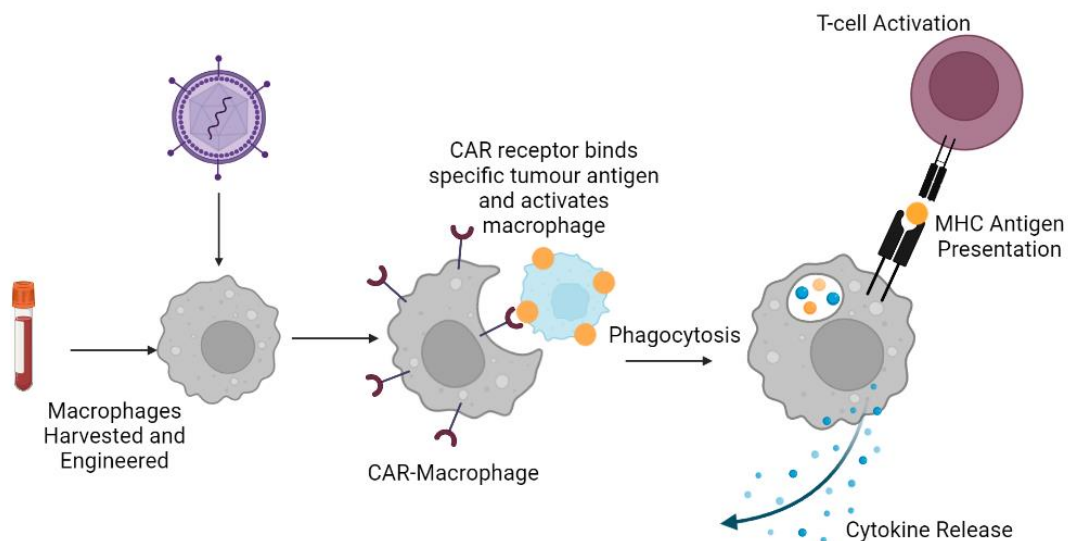


**Figure 2. CAR-Macrophage Function.** Macrophages are harvested and generically engineered to express CAR receptors (maroon). These receptors bind specific tumour antigens (yellow) and upon binding activate the macrophage. The activate macrophage can undergo several different inflammatory processes: 1) phagocytosis of the tumour cells 2) cytokine release and 3) antigen presentation leading to T-cell activation. Figure created in Biorender.

### 1.3.4 Monoclonal Antibodies and Antibody Recruiting Molecules

Monoclonal antibodies (mAbs) represent a popular class of immunotherapeutic that has been used in the clinic since the 1980s.<sup>69,70</sup> Immunotherapeutic mAbs have been engineered to specifically bind a tumour surface marker. They are produced from B-cells that are clones of a single parent cell and therefore each antibody molecule has

the same binding affinity for the antigen. mAb immunotherapeutic function is primarily via triggering innate immune responses such as antibody-dependent cellular phagocytosis (ADCP) and antibody-dependent cellular cytotoxicity (ADCC). The antibodies have a Fab region that binds the tumour antigen with high specificity. They also have an Fc region that can bind and activate immune receptors, for example CD64 on macrophages, to engage a macrophage to the tumour site and promote anti-tumoural immune activity. While mAbs have seen great success in the clinic, they still suffer from limitations. mAbs have difficulty diffusing into solid tumours due to their large size and often require large doses. Further, mAb can be immunogenic, leading to both immune targeting and clearance of the therapeutic mAbs, as well as toxic side effects.<sup>71</sup>

Antibody-recruiting molecules (ARMs) are a promising class of “proximity inducing” small molecule therapeutics.<sup>72</sup> ARMs contain an immune binding domain that binds a hapten specific endogenous serum antibody and a tumour binding domain that binds a cancer cell surface protein (Figure 1). This results in the activation and recruitment of an immune cell to the cancer surface where the macrophage can clear cancerous cells via immune mechanisms such as ADCP or ADCC. A study has reported on the development and characterization of an ARM targeting prostate-specific membrane antigen (PSMA). These ARMs contained a dinitrophenyl (DNP) group that could bind endogenous anti-DNP antibodies and successfully complex them with LNCaP cells expressing PSMA. Further, these ARMs could mediate antibody-dependent killing of the LNCaP cells.

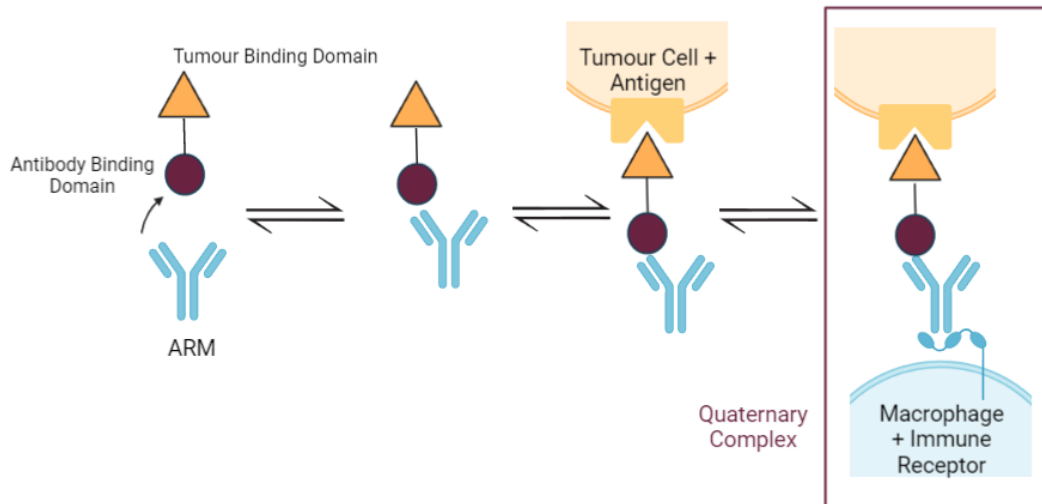


**Figure 3. Schematic Illustrating Antibody Recruiting Molecule Function.** The ARM contains a tumour binding domain (yellow triangle) that reversibly binds a tumour surface protein and an immune binding domain (red circle) that reversibly binds an endogenous anti-DNP antibody. This recruits antibodies to the tumour surface (yellow). The antibodies can then bind and activate immune receptors on the surface of macrophages (blue) to form a quaternary immune complex, leading to ADCP and ADCC of the tumour cells. Figure created in Biorender.

Our group found that ARM anti-cancer activity is limited by the ability of ARMs to form a quaternary complex with the immune cell receptor, antibody and cancer cell surface. Conditions that drive dissociation of this quaternary complex (such as low binding affinity, low antibody concentrations, and clearance) negatively affect ARM anti-cancer efficacy *in vitro* and likely *in vivo*. Because of this, covalent ARMs (cARMs) have been developed that irreversibly link the ARM to the antibody and simplifies the quaternary binding equilibria into a ternary one (Figure 2).<sup>73,74</sup> cARMs differ from ARMs by incorporation of an immune labelling domain that contains a proximity labelling chemical warhead. Once the cARM binds to the antibody, the chemical warhead covalently and irreversibly links to a nucleophilic residue on the antibody surface held in proximity. In this way, the reversible antibody-ARM binding equilibria no longer needs to

be considered for efficacy. In comparison studies, cARMs have shown a marked increase in both target immune recognition and therapeutic efficacy relative to ARMs. However, cARM efficacy is still limited by the affinity of the antibody for the immune receptor and thus are still affected by many of the limitations faced by ARMs and therapeutic antibodies.

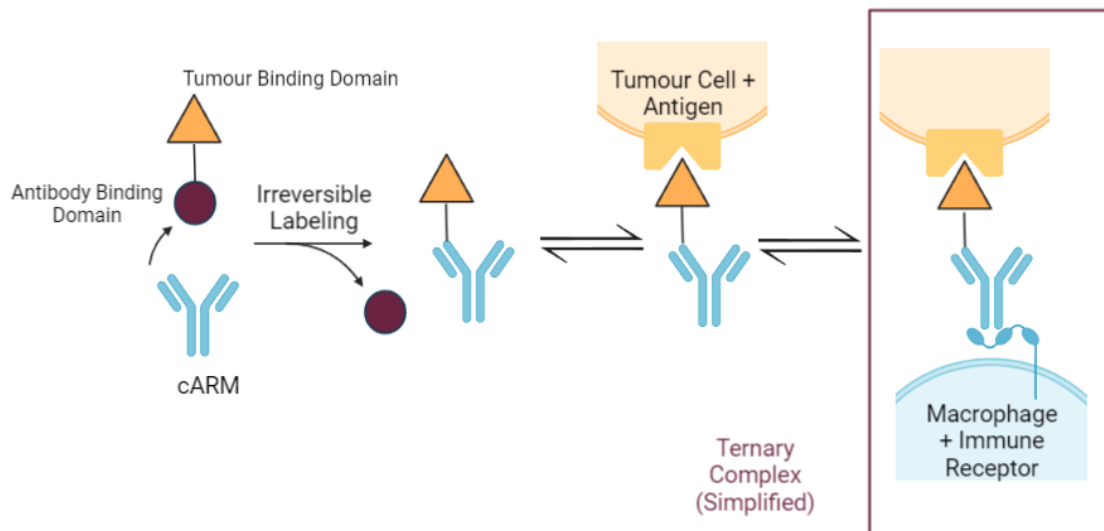


**Figure 4. Covalent Antibody Recruiting Molecules Simplify Complex Formation.** The cARM contains a tumour binding domain (yellow triangle) that binds a tumour surface protein and an immune binding domain (red circle) that binds an endogenous anti-DNP antibody. The cARM can irreversibly label the antibody via a chemical warhead in the immune labelling domain, simplifying the quaternary immune complex into a ternary immune complex. Figure created in Biorender.

## 1.4 Designing Covalent Immune Programmers (CIPs)

### 1.4.1 CIPs: Direct Activating Receptor Labeling Improves on Previous Technologies

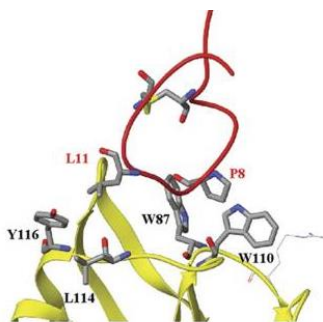
In this project, we aim to develop a novel macrophage immunotherapeutic method by chemically programming macrophages through direct covalent immune

receptor engagement. This method builds on some of the limitations of the strategies discussed previously. ARM and cARM anti-tumour efficacy are limited by the affinity of the antibody to the immune receptor. To address this, we wanted to investigate how direct covalent engagement of the immune receptor and elimination the antibody-immune receptor binding equilibria impacts immune activation and anti-cancer therapeutic efficacy. Doing so also prevents the need for antibodies which can increase solid tumor penetration and additionally tighten the immune synapse. Further, a limitation of current metabolic glycoengineering approaches that attach a tumour targeting molecule onto the macrophage surface is the lack of immune cell activation required for ADCP or ADCC. We hypothesized that by directly targeting and labelling an activating receptor on the macrophage surface, we can induce an anti-tumoral immune response without the need for the addition of other signalling proteins or drugs.

We chose to target CD64 as our immune activating receptor of choice. CD64 is an Fc receptor expressed on the surface of all macrophages that binds IgG with relatively high affinity.<sup>40</sup> Its stimulation is responsible for activation of a macrophage's pro-inflammatory response and is known to promote phagocytosis and the production of reactive oxygen species and pro-inflammatory cytokines. Notably, TAMs have been observed to exhibit an anti-tumour response with CD64 stimulation.<sup>75</sup> This makes CD64 a great receptor to target for directing macrophage activity to tumour cells. CD64 binds the Fc region of IgG antibodies with high affinity.<sup>40</sup> To target these receptors, a peptide that was designed to mimic binding between CD64 and IgG1 (its tightest binding endogenous ligand), called cyclic peptide 33 (cP33), was used.<sup>76</sup> Modeling done by Bonetto et al showed two possible conformations of cP33 that bound to similar sites of

CD64 (Figure 5). cP33 is a 16 residue long cyclic peptide that has been shown in literature to trigger superoxide bursts in monocytes, illustrating successful stimulation of CD64. The sequence of the peptide is: V-N-S-C-L-L-L-P-N-L-L-G-C-D-G-D (Figure 6).

**A.**



**B.**

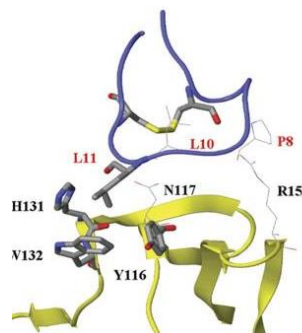


**Figure 5. Molecular modelling of cP33 peptide complexed to CD64.** cP33 peptide is in red. CD64 is in yellow and binding interface residues are denoted in gray. Figure taken from reference 69.

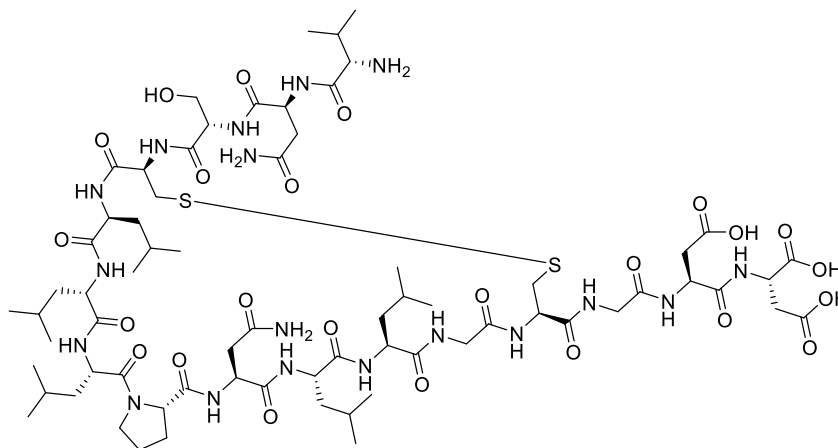


**Figure 6. Structure of cP33 peptide.** The sequence of cP33 is V-N-S-C-L-L-L-P-N-L-L-G-C-D-G-D. The peptide is cyclized via a disulfide bridge between the two cysteines in the sequence. Figure made in ChemDraw.

We have developed and characterized covalent immune programmers (CIPs), which are molecules that contain a “immune binding domain” and a “tumour binding domain” (Figure 7). The immune binding domain binds and activates the pro inflammatory receptor CD64 on the macrophage surface via the cP33 peptide. It also contains a sulfonyl fluoride exchange chemistry (SuFEx) electrophile which serves as a proximity-induced chemical warhead that covalently labels the receptor once bound. The tumour targeting domain contains a ligand that binds a specific tumour antigen known to be upregulated on tumour cells. The identity of this molecule can range from a small molecule to an antibody and helps the CIP recognize the tumour cell. Once the CIP is attached to the activating receptor, the tumour targeting domain can promote macrophage tumour engagement and stimulate tumoricidal function. In this way, CIPs can ‘re-program’ target endogenous macrophages, such as TAMs, to eliminate tumour cells through direct activating receptor labeling.

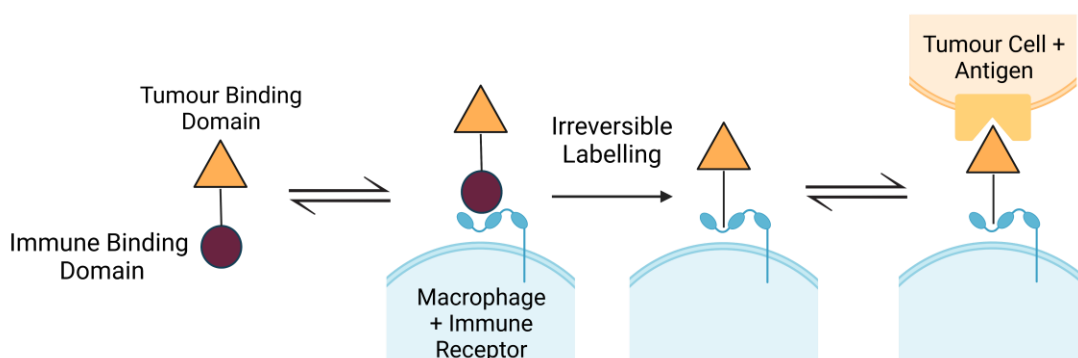


**Figure 7. Schematic illustrating covalent immune programmer function.** The cP33 peptide on the CIP binds to CD64 on macrophages. The affinity labelling chemical warhead then reacts with nucleophilic residues on CD64 to covalently link the CIP and the receptor. The tumour targeting domain can direct macrophage anti-tumoural function towards the tumour cell. Figure made in Biorender.

### 1.4.2 Sulfonyl Fluoride Exchange Chemistry (SuFEx)

We chose to use sulfonyl fluoride exchange (SuFEx) click chemistry as our chemical warhead in the design of our CIPs. SuFEx chemistry involves the reaction of a  $\text{SO}_2\text{F}$  moiety with a nucleophile and relies on the properties of the fluoride-sulfur(IV) bond as well as the unique hydrogen bonding abilities of fluoride (Figure 8).<sup>77</sup> This allows for the formation of a covalent bond between the attacking nucleophile and the SuFEx sulfur in the CIP under specific conditions, dependent upon the stabilization of the fluoride ion leaving group. Notably, because the fluoride ion is stabilized by water, this reaction is promoted in aqueous conditions.

SuFEx chemistry has many advantages over previously labeling chemistries used in the lab, such as acyl imidazole.<sup>78,79</sup> Most importantly, it is more hydrolytically stable and can react with diverse amino acid nucleophiles (Tyr, Lys, Ser, Thr, His, and Cys). SuFEx chemistry is also thermodynamically stable, resistant to reduction and proceeds without the formation of fluorinated by-products.

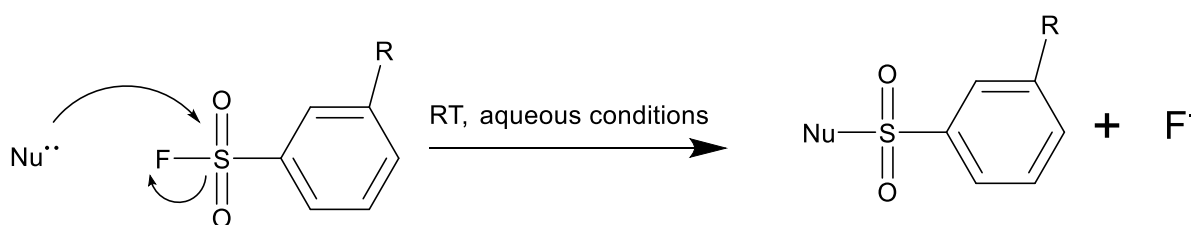


**Figure 8. SuFEx reaction mechanism.** Mechanism outlining how the  $\text{SO}_2\text{F}$  SuFEx group in CIPs reacts with nucleophiles to form a reactive linkage. Figure made in Chemdraw.

### 1.4.3 Tumour Targeting Domains

Urokinase plasminogen activator receptor (uPAR) is a glycolipid-anchored receptor that mediates processes such as extracellular matrix (ECM) remodeling and cell motility in the context of tissue modeling, inflammation or wound healing.<sup>80-82</sup> It is involved in pathways that trigger the activation of proteases that lead to ECM remodeling.<sup>80</sup> It is also involved in the activation of kinases that trigger cellular processes such as cell migration, adhesion, proliferation and angiogenesis.<sup>82</sup>

uPAR is an attractive target for cancer immunotherapeutics because it is highly expressed in tumour tissues.<sup>82,85</sup> High uPAR expression is associated most with solid tumour tissues, such as gliomas. uPAR expression is also observed on stromal cells in the tumour microenvironment such as vascular endothelial cells, TAMs, and tumour associated fibroblasts.<sup>85</sup> In contrast, it is rarely expressed on healthy tissue, reducing the risk of off-targeting effects. Further, many studies have shown that uPAR facilitates tumour progression and plays a role in tumour metastasis, invasion, angiogenesis, and multidrug resistance.<sup>80</sup> As such, uPAR expression on tumour cells is often associated with poor clinical outcomes.

A previous study has identified a peptide known as AE133 that can bind uPAR with high affinity.<sup>86</sup> Our project chose to use a modified version of this peptide as the tumour targeting domain of the CIPs. In this way, we can target and treat a wide variety of different tumour types that over-express uPAR. The sequence of this peptide is: GSGGD-Cha-F-s-r-A-L-W-S, where lowercase denotes d-amino acids (Figure 9).

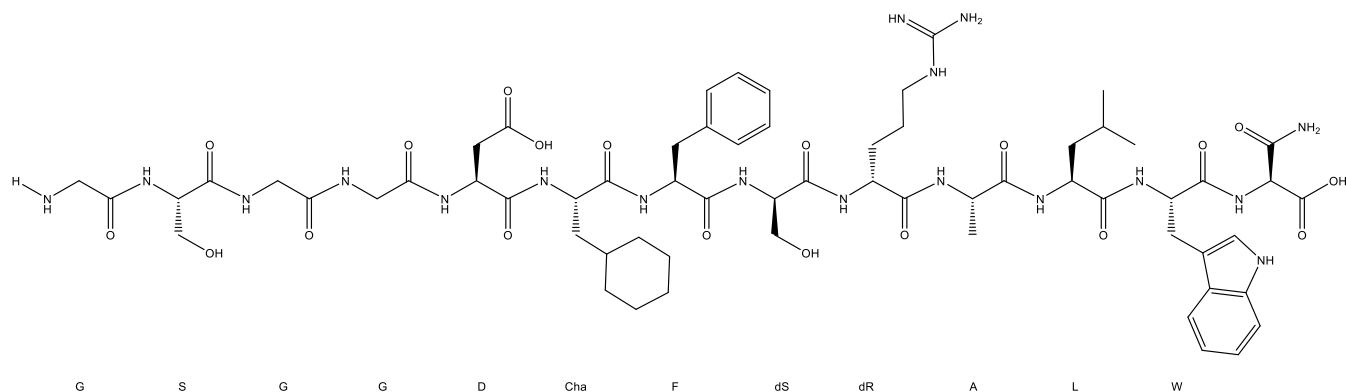


**Figure 9. Modified AE133 Peptide Structure.** The sequence of the modified AE133 peptide used to synthesize CIPs that can target and bind uPAR over-expressing tumour cells is: GSGGD-Cha-F-s-r-A-L-W-S, where lowercase denotes d-amino acids. The c-terminus is amidated. Figure created in ChemDraw.

## 1.5 Project Objectives

The objective of my project is to synthesize and characterize a novel immunotherapeutic, known as covalent immune programmers (CIPs), that uses direct activating receptor covalent labeling to program macrophages to target and eliminate tumour cells. We aim to show that CIPs can specifically label CD64 on the surface of immune cells and that this labeling can mediate an immune response. We hypothesize that direct activating receptor labeling will be more effective than antibody-mediated methods due to the elimination of the Fc receptor-antibody binding step and simplification of the binding equilibria. We also hypothesize that covalent labelling will increase anti-tumoral efficacy and tumour engagement compared to a non-covalent analog similar to the cARM studies discussed previously.

## 2. Materials and Methods

### 2.1 Synthetic Methods

#### **2.1.1 Solid phase peptide synthesis general procedures**

The peptides were synthesized using standard Fmoc-based solid-phase peptide synthesis (SPPS) using a CEM Liberty Blue Automated Microwave Peptide Synthesizer. The synthetic method was based on the manufacturer's suggested protocols based on a 0.1 mmol scale unless otherwise specified. Amide coupling reactions were performed at 40 °C for 10 minutes to decrease aspartimide formation. The deprotection solution used was 20% piperidine with 0.1M oxyma in DMF. The activator solution used was 1M DIC in DMF and the activator base used was 1M oxyma in DMF. The resin used was Rink Amide resin 100-200 mesh (Novabiochem, cat. # 8550010001), resulting in an amide moiety at the c-terminus after cleavage of the peptide off resin instead of a traditional carboxylic acid.

Peptide cyclization (if applicable) was done on resin using Fmoc-Cys-Mmt residues. The Mmt group was selectively deprotected using 0.2% TFA in DCM. 25 mM NCS in DMF was used to facilitate disulfide bridge formation via oxidation on synthesizer. The beads were then gently agitated in DMF for 3 hours to push disulfide bridge formation to completion. N-terminal acetylation (if applicable) was done on resin via reaction with 10% acetic anhydride in DMF.

After SPPS, the resin was washed with DCM and dried using vacuum filtration. The peptide was cleaved from the resin using a 95:2.5:2.5 solution of TFA:H<sub>2</sub>O:TIPS. The cleavage solution was gently agitated for 3 hours before the resin was filtered using vacuum filtration. The filtrate was collected in a 50 mL conical tube and 45 mL of cold

Et<sub>2</sub>O was added to it. The solution was centrifuged for 15 minutes at 3000 rpm and the supernatant was decanted. The pellet was resuspended in a 3 mL 1:1:1 solution of DMF:ACN:H<sub>2</sub>O. The peptide was purified using reverse-phase HPLC with a ThermoFisher DIONEX UltiMate 3000 UHPLC+. A C18 column (Eclipse XDB-C18, 3.5 μm, 2.1 X 100 mm) and a gradient of 95:5 to 5:95 H<sub>2</sub>O (0.1% formic acid):ACN (0.1% formic acid) was used. The HPLC fractions were checked for the presence of the peptide using LCMS with a LTQ Orbitrap XL system using a 5 minute gradient of 95:5 to 5:95 H<sub>2</sub>O (0.1% formic acid):ACN (0.1% formic acid). The desired HPLC fractions were pooled and lyophilized to give the final product as a white powder.

### **2.1.2 Covalent cP33 synthesis**

The SuFEx covalent warhead was selectively installed at specific positions on the peptide by including a Lys-Dde (Chem Impex, cat. # 03718) at the target site during SPPS. After the entire peptide is synthesized on resin, the Dde protecting group is orthogonally deprotected using a 2% hydrazine monohydrate in DMF solution. The SuFEx warhead is then installed by coupling 3-(fluorosulfonyl)benzoic acid (Millipore Sigma, cat. # ALD00038) to the deprotected amine using standard SPPS conditions. The N-terminus CIP analog coupled 3-(fluorosulfonyl)benzoic acid directly to the free n-terminus amine instead.

### **2.1.3 AE133-DBCO synthesis**

The AE133 uPAR binding peptide was synthesized using the standard SPPS procedure outlined previously. Instead of a 1:1:1 solution of DMF:ACN:H<sub>2</sub>O, the crude peptide pellet was resuspended in 100% DMSO prior to purification. The peptide (5 mg,

0.0003 mmol) was dissolved in 400  $\mu$ L DMF. DBCO-NHS (6 mg, 0.0015 mmol) and DIPEA (5  $\mu$ L, 0.003 mmol) was added to the solution. The solution was left stirring for 24 hours at room temperature. The DMF was removed under a nitrogen stream and the resultant yellow oil was dissolved in DMSO. The product was purified using reverse-phase HPLC with a ThermoFisher DIONEX UltiMate 3000 UHPLC+. A C18 column (Eclipse XDB-C18, 3.5  $\mu$ m, 2.1 X 100 mm) and a gradient of 95:5 to 5:95 H<sub>2</sub>O (10 mM ammonium formate):MeOH (10 mM ammonium formate) was used. The HPLC fractions were checked for the presence of the product using LCMS with a LTQ Orbitrap XL system using a 5 minute gradient of 95:5 to 5:95 H<sub>2</sub>O (0.1% formic acid):ACN (0.1% formic acid). The desired HPLC fractions were pooled and lyophilized to give the final product as a white powder.

#### **2.1.4 Installation of reporter molecules or the tumor targeting domain**

All cP33 peptide analogs had an azide incorporated into its sequence that was used to attach targeting domains or reporter molecules containing DBCO moieties through a strain promoted alkyne azide click (SPAAC) reaction between the DBCO and the azide. CIP-biotin was synthesized using DBCO-PEG4-biotin (Broadpharm, cat. # BP-22295). CIP-A647 was synthesized using AZDye 647 DBCO (Click Chemistry Tools, cat # 1302-1). CIP-AE133 was synthesized using AE133-DBCO (synthetic procedure described previously).

All SPAAC reactions were done using a 1:1 ratio of azide:DBCO at 100  $\mu$ M in PBS. The reaction was allowed to run for three hours stirring at room temperature. Complete formation of the product was monitored via LCMS with a LTQ Orbitrap XL

system using a 5 minute gradient of 95:5 to 5:95 H<sub>2</sub>O (0.1% formic acid):ACN (0.1% formic acid).

## 2.2 Fluorescent SDS-PAGE

### 2.2.1 General fluorescent SDS-PAGE procedures

All SDS-PAGE gels were run using 4-20% gradient acrylamide gels (Thermo Scientific, cat. # XP04200BOX). Prior to loading, samples were reduced using 2X Laemmli buffer (Sigma-Aldrich, cat. # S3401-1VL) and boiled at 95 °C for 5 minutes. 20 µL of each sample was loaded onto the gel. A 10-250 kDa protein standard ladder (Bio-Rad, cat. # 1610363) was also loaded on each gel. The gels were run on an Invitrogen Mini Gel Tank (Invitrogen, cat. # A25977) that was covered with aluminum foil to reduce exposure to light. Gels were run initially at 90 volts for 15 minutes followed by 45 minutes at 120 volts. After, gels were washed 2X with water and fluorescence signal was imaged using a Cytiva Amersham Typhoon Biomolecular Imager. The Cy5 channel was used for imaging. Gels were then placed in EZBlue Gel Staining Reagent (Sigma Aldrich, cat. # G1041-500ML) for three hours for protein staining. The gels were then de-stained in water for 3 hours. The protein stain was imaged using a Li-Cor Odyssey CLx Imager.

### 2.2.2 CIP specificity SDS-PAGE assay

1.6 µM of CIP labeled with fluorescent AZDye 647 (CIP-647) was incubated with 800 nM of target protein for 7 hours in PBS at room temperature. The proteins used include human CD64 (ACROBiosystems, cat. # FCA-H52H1), murine CD64 (ACROBiosystems, cat. # CD4-M5227), human CD16 (ACROBiosystems, cat. # CD8-

H52H4) and 5% v/v human serum (Thermo Fisher, cat. # H4522). After incubation, the samples were run on SDS-PAGE gel using the procedure described previously.

### 2.2.3 CIP kinetics SDS-PAGE assay

1.6  $\mu\text{M}$  of each CIP analog labeled with fluorescent AZDye 647 (CIP-647) was incubated with 800 nM of human CD64 (ACROBiosystems, cat. # FCA-H52H1) in PBS at room temperature for varying amounts of time. The SDS-PAGE gel was run and fluorescence was measured according to the general SDS-PAGE protocol described above. The mean fluorescence intensity of each band was determined by measuring the band intensity using ImageJ. The mean fluorescence intensity of each band was converted to fraction labeled by comparing the ratio of the fluorescence intensity of each band to the fluorescence intensity of the band of the 48 hour sample which is assumed to be 100% labeled. A plot of time versus fraction labeled was created and an observed rate constant ( $k_{\text{obs}}$ ) was derived from the plot using the 'one-phase' association equation in GraphPad Prism 9 (Equation 1).

$$\text{Fraction Labeled} = \text{Fraction Labeled}_{t=0} + (\text{Plateau} - \text{Fraction Labeled}_{t=0}) \times (1 - e^{(-k_{\text{obs}} \times \text{time})})$$

**Equation 1.  $k_{\text{obs}}$  derivation equation.** Taken from the 'one-phase' association equation in Graphpad Prism 9.

## 2.3 MALDI

5.4  $\mu\text{M}$  of human CD64 (ACROBiosystems, cat. # FCA-H52H1) and either an equimolar or 10X excess amount of CIP-azide was incubated together in PBS at room temperature for 24 hours. An 'unreacted' 0-hour sample where the CIP was not given time to react was also prepared. The excess unreacted CIP and salts were removed

using a Zeba Spin Desalting Column 7K MWCO (Thermo Fisher, cat. # 89882). The samples were stored on ice and given to Dr. Yang Yang at the McMaster Biointerfaces Institute (McMaster University, Canada) for MALDI analysis.

## 2.4 Aqueous Stability Studies

1 mM of each CIP analog was incubated in PBS at room temperature. At specific time points, an aliquot would be taken from the sample and analyzed using LC-MS with a BRUKER MicroTOF II mass spectrometer with a 20 minute gradient of 95:5 to 5:95 H<sub>2</sub>O (0.1% formic acid):ACN (0.1% formic acid).

## 2.5 Bio-layer Interferometry Binding Assays

The experiment was conducted using an Octet Red96 (Sartorius) with the temperature set at 25 °C, the RPM set at 1000 and the acquisition rate set at 5 Hz. A volume of 200 µL of each solution was loaded into a black flat-bottom 96-well plate (Grenier). Streptavidin probes from Sartorius were placed in 1X Octet Kinetics Buffer (Sartorius, cat. # 18-1105) for 20 minutes prior to experiment for wetting. The experiment begins by placing the streptavidin probes in 1X Octet Kinetics Buffer for 3 minutes to establish a baseline. Biotinylated human CD64 (ACROBiosystems, cat. # FCA-H82E8) was then loaded onto the probes by placing the probes in a 100 nM CD64 in 1X Octet Kinetics Buffer solution for 3 minutes. Next, the probes were placed in 1X Octet Kinetics Buffer for 30 seconds to re-establish a baseline. The probes were then placed in a pre-equilibrated solution of 500 nM uPAR (ACROBiosystems, cat. # UPR-H5226) and 500 nM of uPAR targeting CIP-AE133 or its non-covalent analog (nCIP-AE133) and association of the CIP-uPAR complex was measured for 10 minutes.

Dissociation of the CIP-uPAR complex was measured by placing the probe in 1X Octet Kinetics Buffer for 5 minutes.

The experiment was repeated with biotinylated uPAR (ACROBiosystems, cat. # UPR-H82E7) loaded on the probes. The association of the CD64-CIP complex was measured by placing the probe in a pre-equilibrated solution of 500 nM CD64 (ACROBiosystems, cat. # FCA-H52H1) and 500 nM uPAR targeting CIP-AE133 or nCIP-AE133.

## 2.6 Cell Surface CD64 Labeling Flow Cytometry Assay

### 2.6.1 General Protocol

U937 monocytes were generously given by Dr. John Valiant (McMaster University, Canada). U937 monocytes were cultured in RPMI media (Fisher Scientific, cat. # 31800089) with 2 mM L-Glutamine (Thermo Fisher, cat. # 25030081), 1% Pen/Strep (Fisher Scientific, cat. # 15140-122), and 10% FBS (Fisher Scientific, cat. # 12484-028). The assay media used was DMEM with 2 mM L-Glutamine (Thermo Fisher, cat. # 25030081), 1% Pen/Strep (Fisher Scientific, cat. # 15140-122), and 10% ultra-low IgG FBS (Fisher Scientific, cat. # A3381901).

Cells were seeded in a 96-well U-bottom plate (Fisher Scientific, cat. # 08-772-17) at 100 000 cells in 200  $\mu$ L per well in assay media and preincubated with varying concentrations of CIP-biotin or its noncovalent analog (nCIP-biotin). IFN $\gamma$  (Fisher Scientific, cat. # PHC4031) at a concentration of 0.1 mg/mL was added to all samples except the 'unactivated cells' conditions to activate the monocytes. The cells were incubated for 24 hours in an incubator at 37 °C and 5% CO $_2$ . For covalency controls, samples were prepared that also contained 10X excess CIP-azide as a competitor. 'Co-

incubated Competitor' samples had the competitor added during the 24-hour incubation whereas 'Post-Labeling Competitor' conditions had the competitor added after the 24-hour incubation. A 'No targeting domain' control was also prepared using CIP-azide molecules that did not have the biotin domain.

After incubation the cells were washed 3X with neat DMEM. The cells were then suspended in 200  $\mu$ L of 1.9  $\mu$ M Vybrant DiD Cell Labelling Solution (Fisher Scientific, cat. # V22887) and incubated (37 °C, 5% CO<sub>2</sub>) for 30 minutes. After, the cells were washed 3X with assay media. The cells were treated with a solution of streptavidin-PE conjugate (ThermoFisher, cat. # 12-4317-87) in PBS on ice for 30 minutes. The concentration of streptavidin-PE used is the same as the initial concentration of CIP-biotin added. The cells were then washed 3X with PBS and resuspended in 100  $\mu$ L of PBS. Plates were placed on ice and all conditions were run on a BD LSRII Flow Cytometer to measure fluorescence intensity on the PE channel. The voltages used were: FSC = 430, SSC = 290, PE =260.

### **2.6.2 Installation of the Biotin Domain Post Cell Surface CD64 Labeling via SPAAC**

The assay was repeated with the biotin domain on the CIP installed after the CIP is covalently labeled CD64 on the monocyte cell surface. Instead of CIP-biotin, cells were pre-incubated with varying concentrations of CIP-azide or its noncovalent analog (nCIP-azide). After the 24-hour incubation, DBCO-biotin (Broadpharm, cat. # BP-22295) at 10X the initial concentration of CIP-azide added was spiked into each sample. The samples were incubated for 3 hours at 37 °C. The cells were washed 3X with assay media and the streptavidin-PE labeling step was performed as outlined in the previous general protocol.

## 2.7 Two-colour Phagocytosis Assay

### 2.7.1 General Protocol

U937 monocytes were generously given by Dr. John Valiant (McMaster University, Canada). U937 monocytes were cultured in RPMI media (Fisher Scientific, cat. # 31800089) with 2 mM L-Glutamine (Thermo Fisher, cat. # 25030081), 1% Pen/Strep (Fisher Scientific, cat. # 15140-122), and 10% FBS (Fisher Scientific, cat. # 12484-028). THP1 cells (ATCC, cat. # TIC-202) were cultured in RPMI media (Fisher Scientific, cat. # 31800089) with 2 mM L-Glutamine (Thermo Fisher, cat. # 25030081), 1% Pen/Strep (Fisher Scientific, cat. # 15140-122), and 10% FBS (Fisher Scientific, cat. # 12484-028). The target YG streptavidin beads used were 6.0 µm Streptavidin Fluoresbrite YG microspheres (Polysciences, cat. # 24157-5).

All flow cytometry experiments were conducted using a BD LSRII Flow Cytometer. DiD stained monocytes were detected in the APC Cy7 channel and YG streptavidin microspheres were detected using the A488 channel. The voltages used are: FSC = 430, SSC = 290, A488 = 260, APC-Cy7 = 410. Successfully induced phagocytosis of the target bead by the monocyte is determined by looking at the population that is double positive for both the fluorescent signal of the monocytes and the fluorescent signal of the bead. %Phagocytosis was calculated by comparing the ratio of successful phagocytosis events to the total number of monocytes using Equation 2.

$$\%Phagocytosis = \left( \frac{\text{double positive events}}{\text{monocyte only events} + \text{double positive events}} \right) \times 100$$

**Equation 2.** Equation for %phagocytosis calculations for the two-colour flow cytometry phagocytosis assay.

### **2.7.2 CIP-biotin streptavidin bead phagocytosis assay**

U937 monocytes were seeded in a 96-well U-bottom plate (Fisher Scientific, cat. # 08-772-17) at 100 000 cells in 200  $\mu$ L per well in assay media and preincubated with varying concentrations of CIP-biotin or its noncovalent analog (nCIP-biotin). The assay media used was DMEM with 2 mM L-Glutamine (Thermo Fisher, cat. # 25030081), 1% Pen/Strep (Fisher Scientific, cat. # 15140-122), and 10% ultra-low IgG FBS (Fisher Scientific, cat. # A3381901). IFN $\gamma$  (Fisher Scientific, cat. # PHC4031) at a concentration of 0.1 mg/mL was added to all samples except the 'unactivated cells' conditions to activate the monocytes. The cells were incubated for 24 hours in an incubator at 37 °C and 5% CO $_2$ . A 'No targeting domain' control was also prepared using CIP-azide molecules that did not have the biotin domain.

After incubation the cells were washed 3X with neat DMEM. The cells were then suspended in 200  $\mu$ L of 1.9  $\mu$ M Vybrant DiD Cell Labelling Solution (Fisher Scientific, cat. # V22887) and incubated (37 °C, 5% CO $_2$ ) for 30 minutes. After, the cells were washed 3X with assay media. 150 000 YG streptavidin microspheres were added to each well in a final volume of 100  $\mu$ L of assay media. The plate was centrifuged at 800 rpm for 2 minutes to pellet cells and placed in a 37 °C 5% CO $_2$  incubator for 1 hour. Plates were placed on ice and all conditions run on flow cytometry to determine phagocytosis using the general procedure described previously.

### 2.7.3 CIP-AE133 uPAR bead phagocytosis assay

THP1 monocytes were washed 3X and resuspended to a concentration of 1 million cells/mL with neat DMEM. The cells were dyed with 5  $\mu$ M Vybrant DiD Cell Labelling Solution (Fisher Scientific, cat. # V22887) and incubated (37 °C, 5% CO<sub>2</sub>) for 30 minutes. After, the cells were washed 3X with assay media. The assay media used was DMEM with 2 mM L-Glutamine (Thermo Fisher, cat. # 25030081), 1% Pen/Strep (Fisher Scientific, cat. # 15140-122), and FBS (Fisher Scientific, cat. # 12484-028). The cells were then aliquoted into a 96-well U-bottom plate (Fisher Scientific, cat. # 08-772-17) at 150 000 cells/well and varying concentrations of CIP-AE133 or its noncovalent analog (nCIP-AE133) were added.

In parallel, YG streptavidin beads were washed 3X in PBS. They were then incubated in a 200 nM biotinylated human uPAR (ACROBiosystems, cat. # UPR-H82E7) solution at a concentration of  $5 \times 10^7$  beads/mL for 1 hour at room temperature. The beads were then washed once in assay media. 150 000 labeled beads were added to each sample well. The final volume for each sample was 100  $\mu$ L in assay media. The plate was centrifuged at 800 rpm for 2 minutes to pellet cells and placed in a 37 °C 5% CO<sub>2</sub> incubator for 1 hour. Plates were placed on ice and all conditions run on flow cytometry to determine phagocytosis using the general procedure described previously.

## 2.8 THP1 NF- $\kappa$ B Activation Reporter Cell Assay

The THP1-NF- $\kappa$ B activation reporter cell assay was done by Dr. Mauro Castellarin (Rullo Lab, McMaster University).

A THP1 NF- $\kappa$ B-Luc2 reporter cell line (ATCC, TIB-202-NFKB-LUC2) that produces luciferase when the NF- $\kappa$ B activation pathway is stimulated was used to assess monocyte activation. THP1 NF- $\kappa$ B-Luc2 cells were cultured in RPMI media (Fisher Scientific, cat. # 31800089) with 2 mM L-Glutamine (Thermo Fisher, cat. # 25030081), 1% Pen/Strep (Fisher Scientific, cat. # 15140-122), and 10% FBS (Fisher Scientific, cat. # 12484-028).

Streptavidin microspheres (Polysciences, cat. # 24158-5) were labeled with CIP-biotin or its nCIP-biotin. The beads were washed 3X in PBS. They were then incubated in a 500 nM CIP-biotin/nCIP-biotin solution at a concentration of  $5 \times 10^7$  beads/mL for 1 hour at room temperature. The beads were then washed once in PBS. The beads were incubated with cells at a 5:1 ratio of bead:cell in media for 24 hours in a 96 well black clear bottom plate (ThermoFisher, cat. # 165305). After 24 hours, luminescence was measured using a TECAN Spark Microplate Reader.

### 3. Results and Discussion

#### **3.1 CIP Design**

Successful CIP design relies on the ability of its immune binding domain to bind an activating receptor specifically and to induce immune effector function. The CD64 binding peptide cP33 was chosen as the immune binding domain. Notably, this peptide has been successfully used in immune recruiting ‘synthetic antibody mimics’ (SyAMs) by Speigel et al.<sup>87</sup> SyAMs also aim to bridge CD64 and tumor antigens on cancer cells, however they are designed to mimic the mechanism of monoclonal antibodies and function through multivalent binding. Monovalent SyAMs were unable to induce phagocytosis of tumor targets. We hypothesize that SyAMs suffer from the same

limitations as monoclonal antibodies or cARMs discussed previously. Introducing covalency, through direct activating receptor labeling, could improve the efficacy of this peptide.

Previous studies in the Rullo lab have demonstrated that cP33 binds CD64 with a  $K_D$  of 52 nM.<sup>88</sup> To synthesize a CIP, the cP33 peptide was modified in two major ways. First, an azide was included at the N-terminus of the peptide to allow for installation of the tumor binding domain using strain promoted alkyne-azide chemistry (SPAAC). An aryl sulfonyl fluoride (SuFEx) chemical electrophile was also installed within the peptide that will react with a nucleophilic residue on CD64 upon binding through “proximity activation” to result in an irreversible covalent bond between CIP and receptor.

### **3.2 CIP Synthesis**

The cP33 peptide was synthesized using standard Fmoc-based solid phase peptide synthesis (SPPS). Previous synthesis of this peptide by other students in the lab have reported the formation of an aspartimide side product, where the carboxylic acid on the aspartic acid residue in the peptide sequence reacts with the nitrogen in the peptide backbone to form a cyclic imide (Figure 10A).<sup>89</sup> The ring can be opened and lead to 4 different products depending on the nucleophile. This phenomenon occurs more frequently when there is a glycine residue next to the aspartic acid residue, as seen in the cP33 peptide.

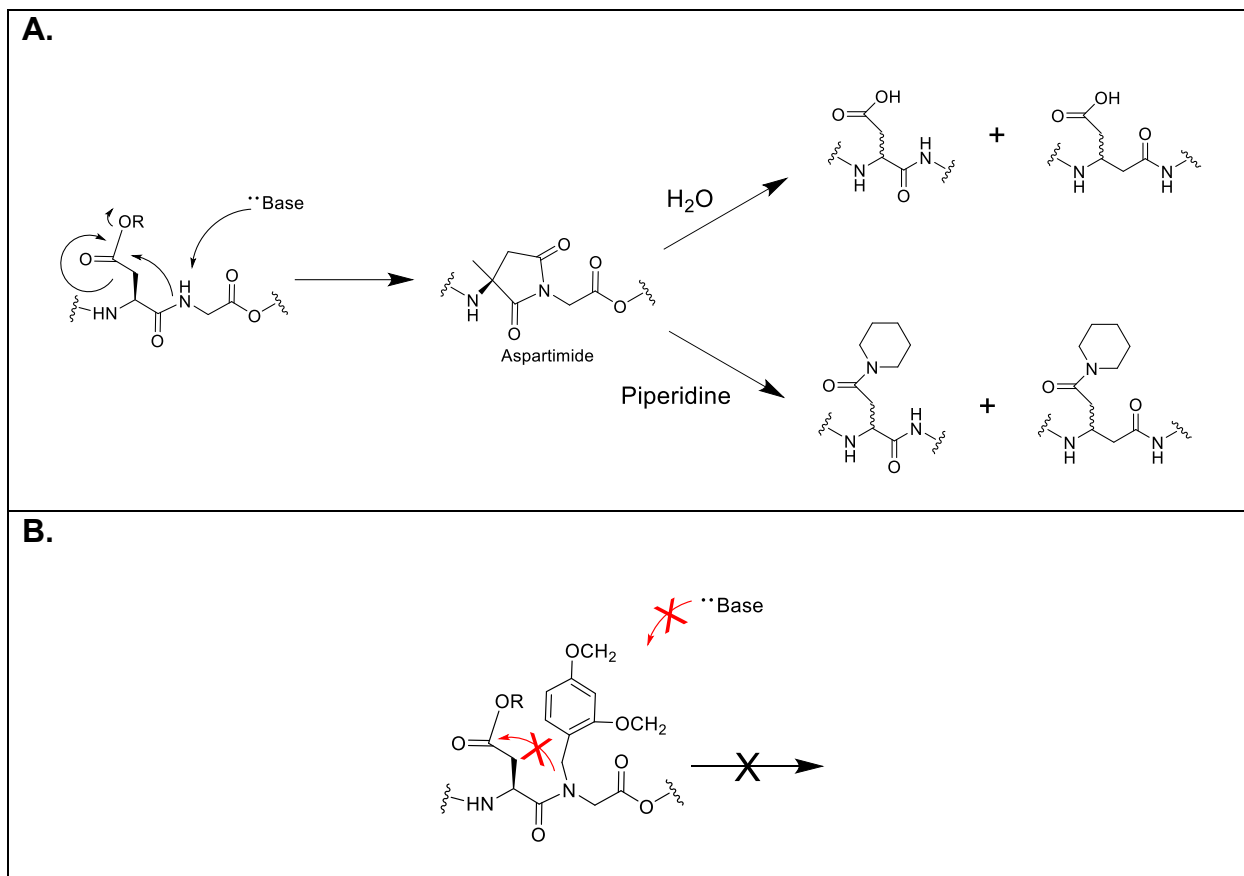


**Figure 10. Aspartimide formation.** A) Mechanism of aspartimide formation and structure of possible side products B) Structure of Asp-Dmb-Gly

To reduce aspartimide formation, the temperature of the amide coupling reaction was lowered from the manufacturer recommended 90 °C to 40 °C as aspartimide formation is favored at high (<45 °C) temperatures.<sup>90</sup> To account for any decrease in coupling efficiency correlated with the lower reaction temperature, the reaction time was increased from 2 minutes to 10 minutes. An Asp-Dmb-Gly dipeptide with an acid-labile 2,4-dimethoxybenzyl (Dmb) protecting group on the backbone nitrogen to prevent reaction with the aspartic acid (Figure 10B) was used.<sup>87</sup> Finally, 0.1M oxyma was added to the deprotection solution, which was shown in literature to decrease aspartimide formation. Oxyma is thought to work as an acidic modifier that reduces the first step of aspartimide formation, the base-catalyzed deprotonation of the aspartyl amide.<sup>91</sup>

The N-terminal azide was installed by coupling a pre-synthesized lysine-azide residue to the N-terminus of the cP33 peptide during SPPS. To assess if the position of the SuFEx chemical electrophile will affect labeling efficacy, we synthesized three different CIP electrophile analogs with the SuFEx located at three different positions within the peptide: the N-terminus (Nt-CIP), the C-terminus (Ct-CIP), and internally (Int-CIP) (Figure 11). The Int-CIP electrophile analog has the SuFEx electrophile replacing the leucine at residue 7. This choice was done based on modeling by an undergraduate student in the lab, Gavin Yuen, which shows that removing the leucine can greatly increase the peptide's solubility. Further, predictive models have shown that when bound, the residue at position 7 is close to many nucleophilic residues in the CD64 binding pocket. A non-covalent analog (nCIP) which did not have the SuFEx electrophile installed was also synthesized for comparison. We hypothesized that nCIP will be less effective than CIP, illustrating a covalent advantage.

The SuFEx electrophile was installed at specific positions by incorporating a Lys-DDE residue at the target position through SPPS (Figure 12). N-[1-(4,4-dimethyl-2,6-dioxocyclohex-1-ylidene)ethyl] (DDE) is a protecting group that can be orthogonally deprotected after complete synthesis of the peptide on resin. SuFEx can then be installed by coupling a 3-fluorosulfonyl(benzoic acid) onto the deprotected amine of the lysine using standard SPPS coupling conditions. The Nt-CIP was synthesized by coupling 3-fluorosulfonyl(benzoic acid) directly to free amine on the N-terminus. The final %yield was approximately 20%. The low yield is likely due to the large size and hydrophobicity of the peptide decreasing SPPS efficiency. The propensity of the peptide

of aggregate also resulted in a significant loss of product in the HPLC column. Appendix 1-3 shows the LC-MS spectra of each purified analog.

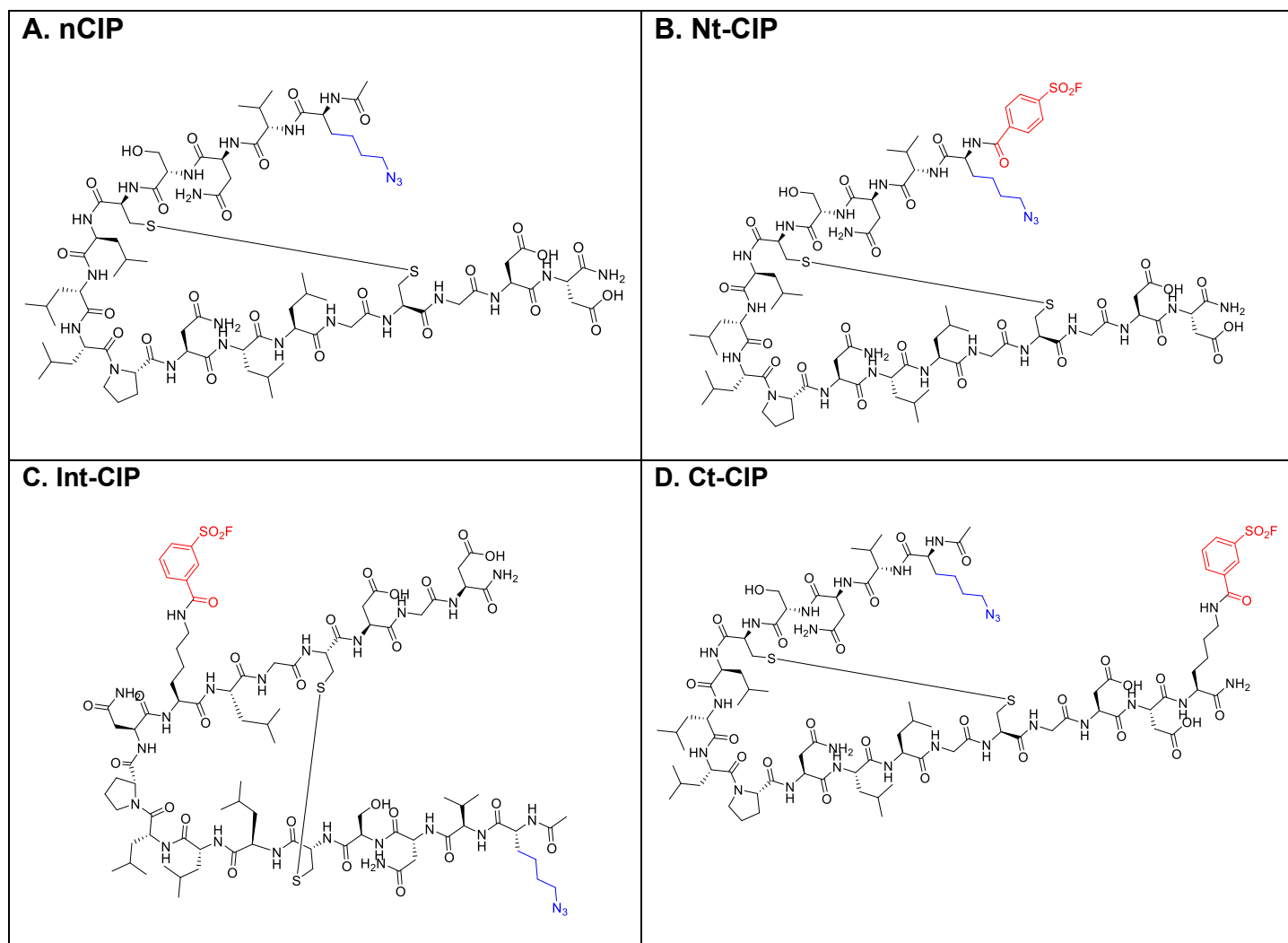


**Figure 11. Chemical structure of CIP analogs.** The SuFEx electrophile is highlighted in red. The azide moiety used to install the tumour targeting domain via SPAAC chemistry is highlighted in blue. A) non-covalent analog of CIP (nCIP) that does not contain a SuFEx covalent electrophile. B) CIP with the SuFEx electrophile on the N-terminus (Nt-CIP) C) CIP with the SuFEx installed internally replacing the leucine at residue 7 (Int-CIP) D) CIP with the SuFEx installed at the C-terminus (Ct-CIP).

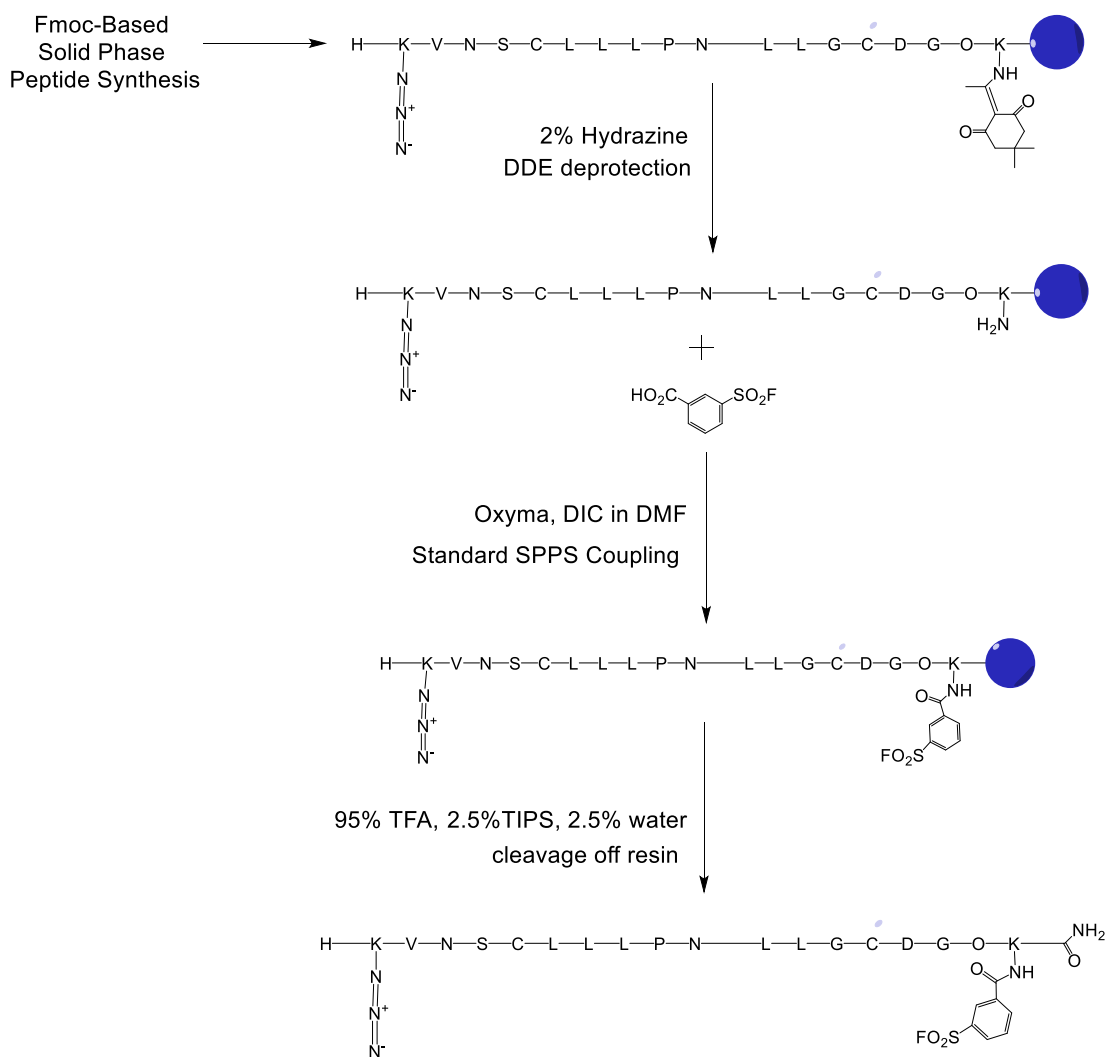
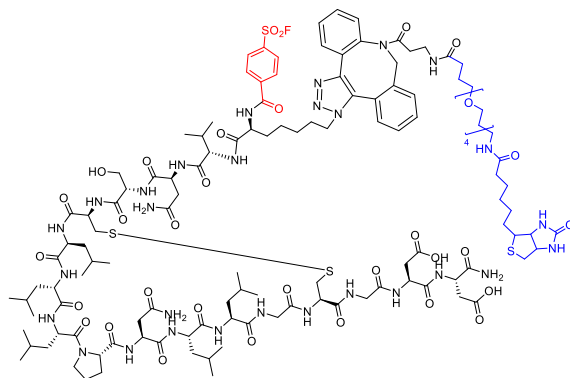


**Figure 12. CIP Synthetic Scheme.**

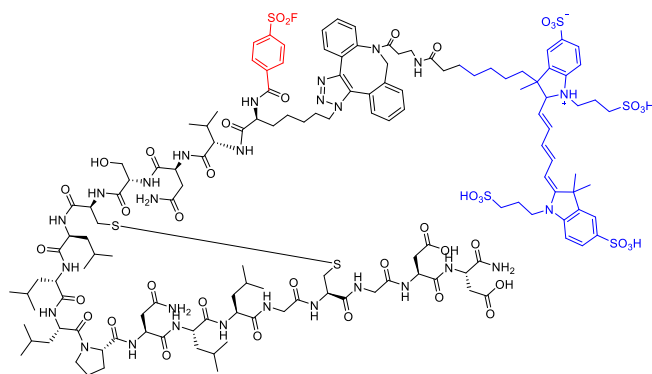
The tumor targeting domain was installed using SPAAC click chemistry after peptide purification as we did not have the large amounts of reagent needed to perform the click on resin. However, future synthesis should consider completing the click reaction during SPPS to improve purity and yield. In this thesis, three different targeting motifs were explored (Figure 13). This first targeting domain installed was a biotin (CIP-biotin). The second CIP targeting analog is a fluorescent version which has a fluorescent AzDye 647 dye as the “targeting domain” (CIP-A647). The final targeting domain is a uPAR binding peptide known as AE133 (CIP-AE133) which can be used in

functional assays to target tumor cells associated with high levels of surface uPAR expression.

### CIP-biotin



### A. CIP-A647



### B. CIP-AE133

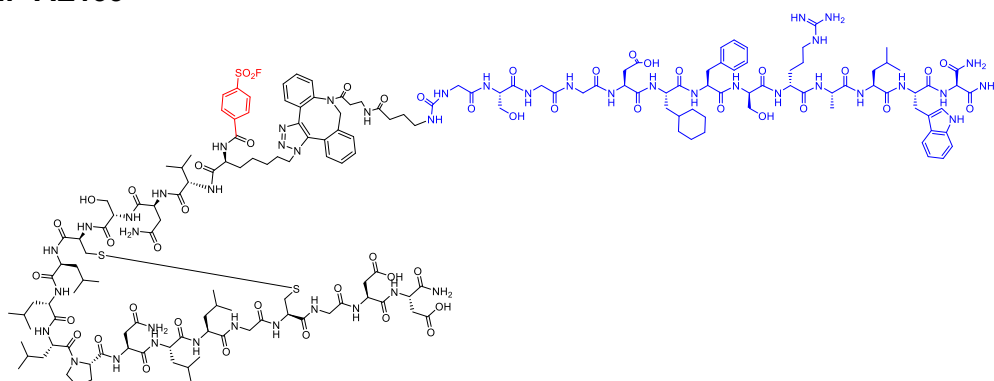


**Figure 13. Chemical Structure of CIP Targeting Analogs.** Nt-CIP is depicted however all three targeting analogs were also made for Ct-CIP and Int-CIP. The SuFEx covalent electrophile is highlighted in red. The targeting domain installed is highlighted in blue and are as follows: A) biotin (CIP-biotin) B) fluorescent dye AzDye 647 (CIP-A647) C) uPAR binding peptide AE133 (CIP-AE133)

### 3.3 CIP can Selectively and Covalently Label CD64 in Solution

We initially synthesized Nt-CIP and characterized its ability to specifically and covalently label CD64 as a proof-of-concept. We first validated this through SDS-PAGE using fluorescently labeled Nt-CIP-A647 (Figure 14). Nt-CIP-A647 (1.6  $\mu\text{M}$ ) and 800 nM of CD64 were incubated for 7 hours in PBS at room temperature. The concentrations chosen were significantly above the  $K_D$  to ensure complete binding. The sample was then run on a reducing SDS-PAGE gel and the fluorescence signal of Nt-CIP-A647 on the gel was imaged. Only Nt-CIP-A647 that has covalently labeled CD64 can remain complexed with CD64 as the gel would disrupt all non-covalent interactions. The CD64 band is highly fluorescent (Figure 14A), which suggests that Nt-CIP-A647 can bind CD64 covalently.

This SDS-PAGE experiment was also conducted with murine CD64; human CD16a, an immune receptor similar to CD64; and 5% human serum. The fluorescence of these protein bands is much lighter than the human CD64 band (Figure 14A), showing that Nt-CIP-A647 preferentially labels CD64. Notably, Nt-CIP-A647 does not appear to label murine CD64, which indicates a high level of specificity as even slight differences between versions of CD64 can affect labeling. The Coomassie stain is much darker for 5% human serum compared to the other proteins showing that there is significantly more protein in the 5% human serum sample (Figure 14B), however its fluorescence signal is still lower than the CD64 sample, further validating CIP labeling specificity.

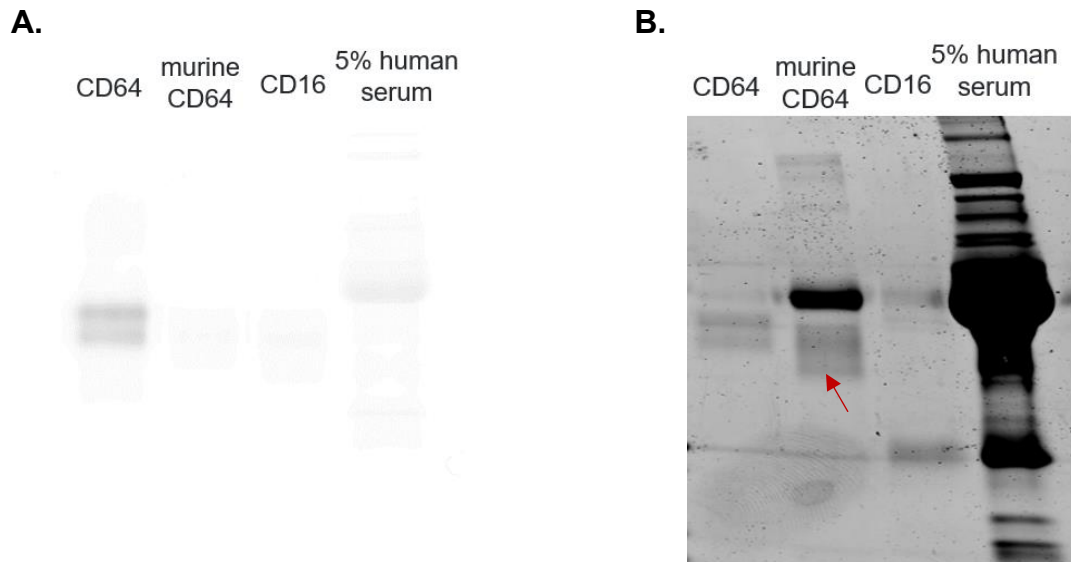


**Figure 14. Nt-CIP *in solution* CD64 labeling specificity.** Fluorescent Nt-CIP-A647 (1.6  $\mu$ M) was incubated with 800 nM of human CD64, murine CD64, CD16 or 5%human serum in PBS for 7 hours at room temperature. A) Detection of fluorescent signal using the Cy5 channel. A darker band correlates to a higher fluorescence signal and more CIP labeling B) Coomassie protein stain showing the relative abundance of each protein on the same gel. The murine CD64 protein band is denoted with a red arrow and the dark band above the murine CD64 band is BSA.

The murine CD64 protein band is the lighter band that is denoted with a red arrow and not the significantly darker band above it. The darker band is BSA that was added to the murine CD64 as a carrier protein for storage stability.

To further validate that CIPs can label CD64 covalently we ran MALDI analysis on an ‘unlabeled’ CD64 sample (Figure 15A) and a sample of 5.4  $\mu$ M CD64 (Figure 15B) that reacted with 54  $\mu$ M Nt-CIP for 24 hours in PBS at room temperature. The mass shift of the CD64 peak from 44416 m/z to 47236 m/z corresponds to the average mass of the peptide covalently linked to CD64. As the MALDI peak represents the average mass of a population, % labeling is calculated by comparing the ratio of the mass shift of the CD64 MALDI peak with the mass of Nt-CIP. The % labeled is over 100%, however some of this discrepancy could be due to slight mass differences in

CD64 between the two samples due to differences in glycosylation pattern. Due to the high concentration and long reaction time, it is also likely that some CIP labeled non-specifically outside of the binding pocket, leading to double labeling of CD64.

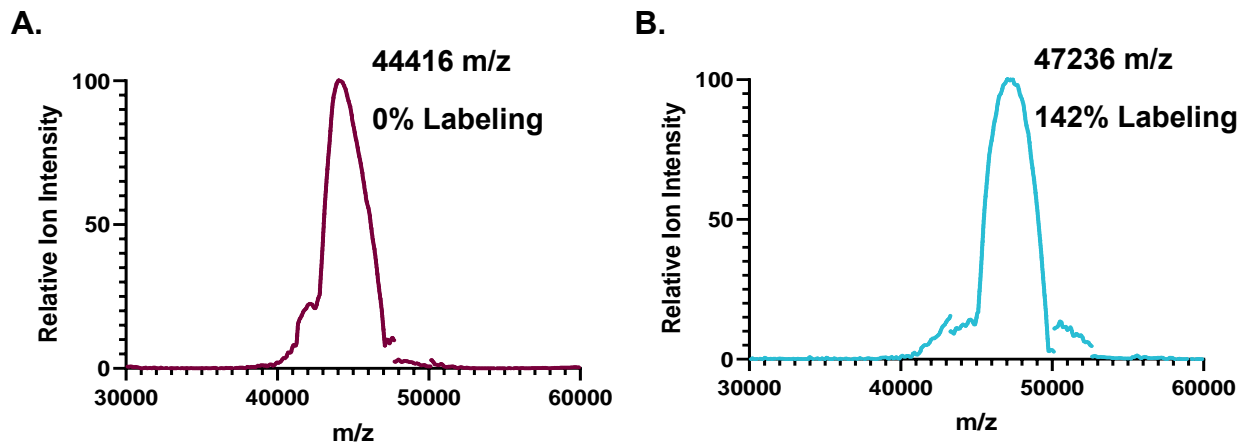


**Figure 15. Nt-CIP CD64 Labeling MALDI Spectra.** A) MALDI spectra of unlabeled CD64. The peak is at 44416 m/z B) MALDI spectra of CD64 reacted with 10X Nt-CIP for 24 hours at room temperature. The peak has shifted from the baseline peak seen in Figure 11A and is at 47236 m/z, corresponding to 142% labeling. % labeling is calculated by comparing the ratio of the mass shift of the MALDI peaks with the mass of Nt-CIP.

### 3.4 CIP can Specifically and Covalently Label CD64 on the Immune Cell Surface

After validating that CIPs can covalently label CD64 in solution, we wanted to investigate if CIPs can label CD64 on the surface of live immune cells. To do this, we pre-labeled IFN $\gamma$  activated U937 monocytes with Nt-CIP-biotin for 24 hours at 37 °C. To measure labeling, cells were then treated with a fluorescent streptavidin-phycoerythrin (streptavidin-PE) reporter molecule. Fluorescence was read using flow cytometry. We chose not to use Nt-CIP-A647 as a direct reporter fluorophore due to the possibility of the fluorescent CIP being internalized. With streptavidin-PE as the reporter molecule, fluorescence directly correlates to the amount of CIP on the surface available to engage a tumor target.

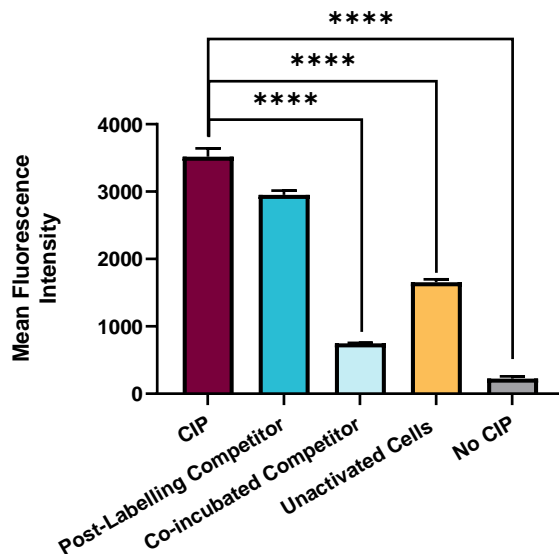
Figure 16A shows successful labeling of CD64 by Nt-CIP-biotin as the mean fluorescence intensity of the labeled cells increased significantly from the baseline fluorescence where no CIP is added. Further, to assess if the labeling is truly covalent, a competitor (10X excess noncovalent CIP with no biotin domain, nCIP-Az) was added after 24-hour incubation of Nt-CIP-biotin with U937s (Figure 16A). The mean fluorescence intensity did not decrease significantly with the addition of the competitor, suggesting that the labeling is irreversible, and the competitor could not outcompete the already labeled Nt-CIP-biotin. However, this data alone is not sufficient to prove covalent labeling as the excess competitor could be binding to non-specific binding sites instead of competing with Nt-CIP-biotin labeling.

To address this concern, competitor was added during the 24-incubation period. The mean fluorescence intensity decreased significantly to almost baseline levels. This confirms that CIP covalent labeling is specific as the competitor outcompeted CIP for the specific binding site rather than be sequestered in off-target sites.

When U937s that were not activated with IFN $\gamma$  were assayed, the fluorescence decreased significantly (Figure 16A). This decrease correlates with the decrease in CD64 expression on the surface of unactivated cells, again supporting that CIP cell labeling is CD64 specific. Figure 16B shows that Nt-CIP-biotin labels CD64 on the surface of immune cells in a concentration dependent manner. Notably, the binding appears to saturate around 500 nM where the fluorescence plateaus. This further validates CIP labeling selectivity as the fluorescence plateau represents when all the specific binding sites are saturated. If binding was non-specific, fluorescence should

continue to increase as the non-specific binding sites prevent labeling from reaching saturation.

A.



B.

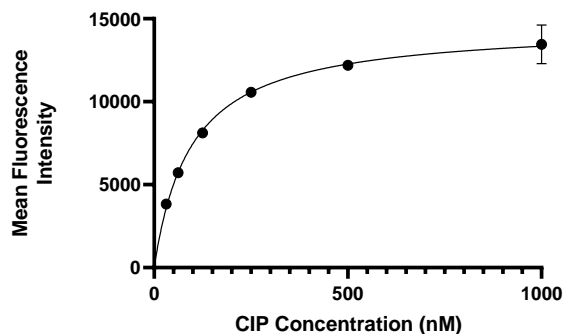


**Figure 16. CIP monocyte cell surface CD64 labeling.** Nt-CIP-biotin was incubated with IFN $\gamma$  activated U937 monocytes for 24 hours. Labeling was assessed by measuring cellular fluorescence using a streptavidin-PE reporter molecule in flow cytometry. A) Labeling at 500 nM Nt-CIP-biotin with competitor controls to assess covalency and unactivated cells to assess CD64 specificity. Error is standard deviation. \*\*\*\* =  $p < 0.0001$  B) Labeling of Nt-CIP-biotin concentration series showing Nt-CIP-biotin labels CD64 on cells in a concentration dependent manner. Error is standard deviation.

### 3.5 Optimizing Covalent Electrophile Position

Once we established that CIPs can covalently label CD64, we wanted to test if changing the position of the electrophile can further increase labeling kinetics. SuFEx reactivity has been shown in literature to be very sensitive to the reaction microenvironment. We hypothesized that changing the environment of the SuFEx electrophile and which binding pocket residues it is positioned close to could greatly affect reaction kinetics.

We again used a fluorescent SDS-PAGE gel assay to measure reaction between CD64 (800 nM) and 1.6  $\mu$ M of CIP-A647 at room temperature in PBS. Aliquots of the reaction were taken and frozen at -80 °C at specific time points before being run on a gel. The fluorescence intensity of each band was used to determine the fraction labeled at each time point by comparing the fluorescence of each time point with the 48h hour time point confirmed by MALDI to be 100% labeled in a 2:1 stoichiometry. Surprisingly all three CIP electrophile analogs showed similar observed labeling kinetics, reaching a fluorescence plateau after 8 hours for all analogs (Figure 17A-C, Table 2).

The intensity of the fluorescence bands at the plateau differs between each CIP electrophile analog (Figure 17). This could be due to a variety of reasons, such as dye quenching in different microenvironments or variation between protein stocks. However, we hypothesized that the less fluorescently intense bands are a result of CIPs degrading into an inactive form. As a result, less CIP is available to label CD64 and less fluorescent CD64 complex is observed in the band fluorescence intensity.

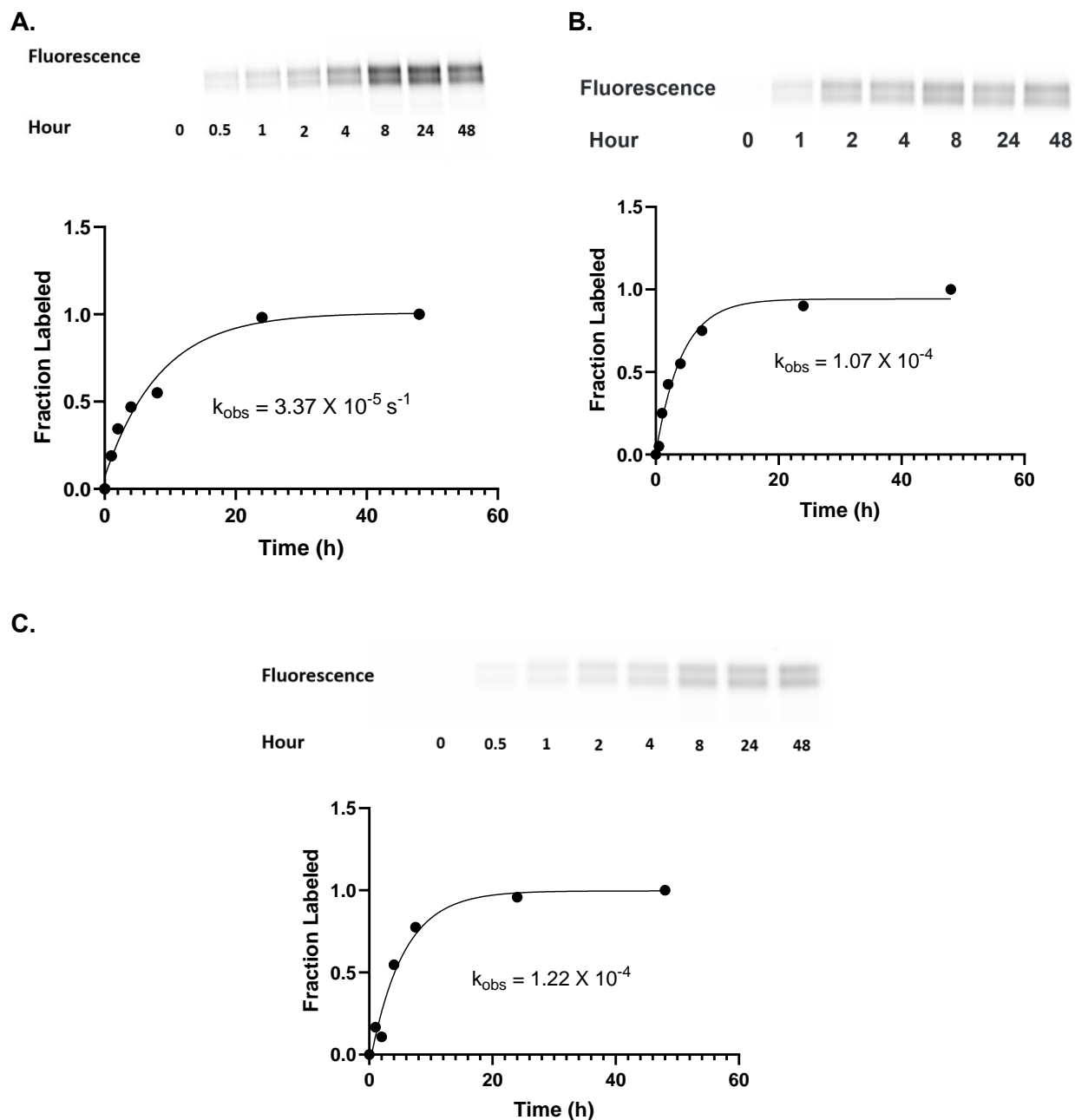


**Figure 17. CIP electrophile analog kinetics.** The fluorescence intensity plateaus by 48 hours, which is assumed to be 100% labeling. The fluorescence intensity of each band was measured and compared as a ratio to the fluorescence intensity of the band at 48 hours to calculate fraction labeled. A) Nt-CIP labeling kinetics.  $k_{obs} = 3.37 \times 10^{-5}$  B) Ct-CIP labeling kinetics.  $k_{obs} = 1.07 \times 10^{-4}$  C) Int-CIP labeling kinetics.  $k_{obs} = 1.22 \times 10^{-4}$

CIP electrophile analog	$k_{obs}$ ( $s^{-1}$ )
Nt-CIP	$3.37 \times 10^{-5}$
Ct-CIP	$1.07 \times 10^{-4}$
Int-CIP	$1.22 \times 10^{-4}$

**Table 2. CIP electrophile analog  $k_{obs}$  labeling rate constants.**

To assess if the fluorescence plateaus observed in the previous experiment are the result of reaction completion or CIP degrading into an inactive form, the aqueous stability of each CIP analog was assessed by LC-MS after incubation for up to 27 hours in PBS. Stability was determined by monitoring the appearance of degradation peaks in the LC-MS spectra. Expected degradation peaks include a -2 mass shift peak, representing hydrolysis of the SuFEx electrophile, and a -19 mass shift peak where the SuFEx electrophile reacts with another amino acid residue on the CIP either intermolecularly or intramolecularly. SuFEx is likely to react with the serine within the peptide sequence. Free cysteine residues that did not successfully form a disulfide bridge could also react with SuFEx.

All three CIP electrophile analogs displayed reasonable stability as all three had a strong intact product peak that remained present over 27 hours. Nt-CIP-Az was the most stable analog as no degradation peaks were observed (Figure 18A). Int-CIP-Az was the least stable and a strong degradation peak was observed by 7 hours. However, an intact product peak was still observed by 27 hours as well (Figure 18C). Ct-CIP-Az stability studies show some degradation product peaks by 27 hours (Figure 18B). While electrophile position does not affect the rate at which the labeling reaction reaches a plateau, it does affect CIP aqueous stability.

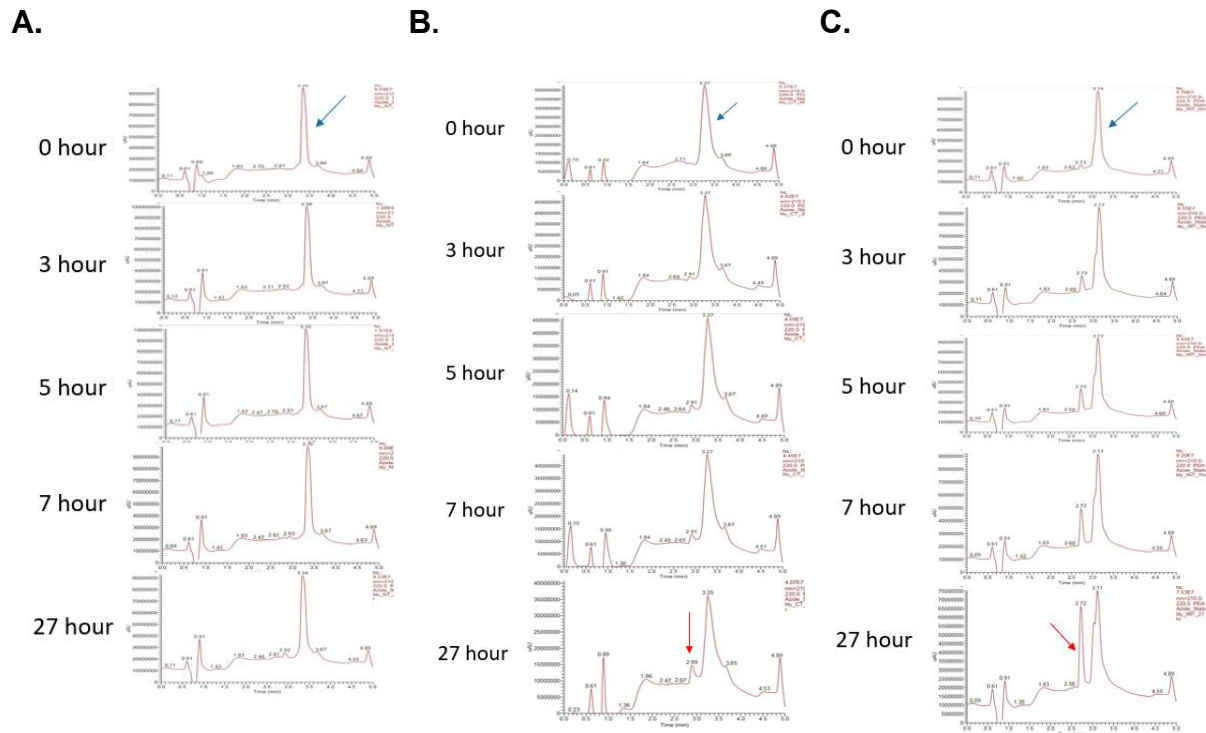


**Figure 18. CIP aqueous stability studies showing the UV trace from LC-MS analysis.** Stability is assessed by monitoring the appearance of degradation peaks (denoted by red arrows). The intact product peak is denoted by blue arrows. A) Stability study for Nt-CIP-Az. The intact product peak elutes at 3.35 minutes. B) Stability study for Ct-CIP-Az. The intact product peak elutes at 3.27 minutes. C) Stability study for Int-CIP-Az. The intact product peak elutes at 3.31 minutes.

Stability can greatly affect the kinetics measured previously as degradation acts as a competitive pathway to labeling. This could result in the kinetics for the least stable analog (Int-CIP-Nt) appearing artificially slower as not all the CIP is available to label. Further, the difference in stability suggests that  $k_{obs}$  cannot be directly compared between the three analogs. The Nt-CIP fluorescence at plateau is significantly more intense compared to Int-CIP fluorescence. This suggests that Nt-CIP labeled more CD64 than Int-CIP. The plateau in intensity for the Int-CIP is likely not due to 100% labeling but rather the result of degradation inactivating most of the CIP and forcing labeling to plateau prematurely.

Finally, we investigated whether changing the position of the SuFEx electrophile would affect the ability of the CIP to label CD64 on an immune cell surface using the same streptavidin-PE reporter flow assay described previously (Figure 19). We observed a significant difference in labeling efficacy depending on the position of the electrophile. Nt-CIP-biotin had a significantly higher mean fluorescence intensity compared to the other analogs and therefore was the most effective at labeling cell-surface CD64. Int-CIP-biotin was the least effective at labeling cell-surface CD64. Labeling efficacy appears to correlate with aqueous stability as the most stable CIP electrophile analog was the most effective at labeling the cell surface. We concluded that the difference in labeling efficacy is due to the more unstable CIPs degrading more quickly into inactive side products rather than due to a difference in labeling rate. Labeling rate may have a more significant affect if Int-CIP was more stable. A significant cause of inactive side product formation is likely the reaction of the serine residue in cP33 with the SuFEx electrophile. The shift in electrophile position could have placed the SuFEx at the ideal distance for intramolecular reaction. To investigate this experimentally, the serine could be replaced by an inert amino acid residue in Int-CIP to see if stability would change.

A noncovalent analog (nCIP) was also tested and showed very little labeling with mean fluorescence intensity at near baseline levels. When compared to Nt-CIP-biotin, the nCIP condition illustrates the importance of covalency to stably engage CD64 on the cell surface. For simplicity, we chose to conduct our remaining studies with Nt-CIP due to its superior stability.

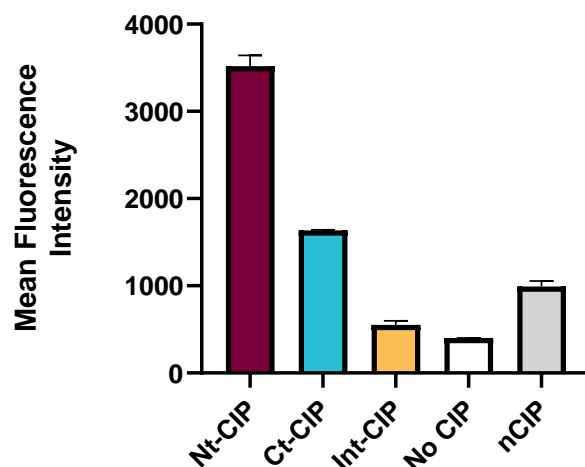


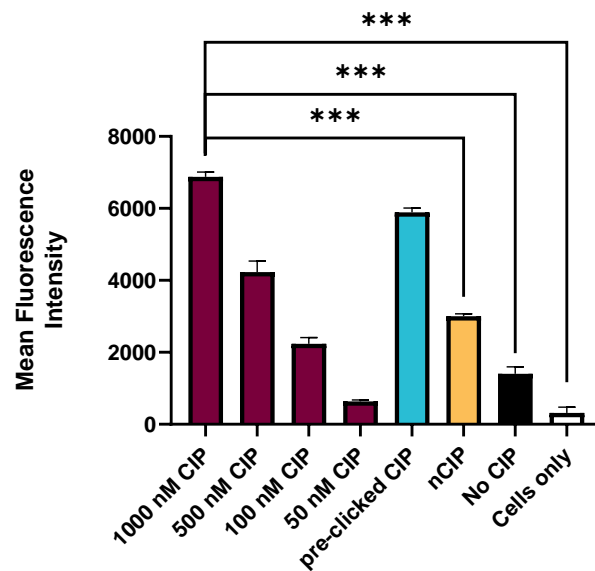
**Figure 19. Covalent electrophile position affects cell surface CD64 labeling.** 80 nM of CIP-biotin was incubated with IFN $\gamma$  activated U937 monocytes for 24 hours. Labeling was measured by measuring the fluorescence of a streptavidin-PE reporter molecule using flow cytometry. Errors are standard deviation.

### 3.6 Tumor Targeting Domains can be Installed on the Immune Cell Surface via CIPs

Previous metabolic labeling approaches to immunotherapy describe functionalizing immune cells by incorporating an unnatural analog sugar biomolecule that has a reactive click handle. As the cells metabolically incorporate the unnatural sugar to the cell surface, a targeting domain can be installed using *in situ* click chemistry.

As an alternative to these metabolic labeling approaches, we tested our CIP strategy for the ability to program a non-engineered macrophage with tumor targeting capabilities. Specifically, we evaluated if a targeting ligand could be site selectively installed on monocyte cell surface CD64 labeled with Nt-CIP-Az. We hypothesized CIPs can be used to label CD64 with click handles, allowing for subsequent bio-orthogonal incorporation of targeting ligands via SPAAC click chemistry directly on the immune cell surface. As a proof-of-concept, we studied the incorporation of DBCO-biotin, in the

context of a modified version of the cell surface labeling flow cytometry assay described above. Here, cells were treated with Nt-CIP-Az for 24 hours at 37 °C followed by treatment with a 10X excess of DBCO-biotin for 3 hours at 37 °C. The ability of DBCO and the azide to react and install biotin on the cell surface was monitored using a streptavidin-PE conjugate.



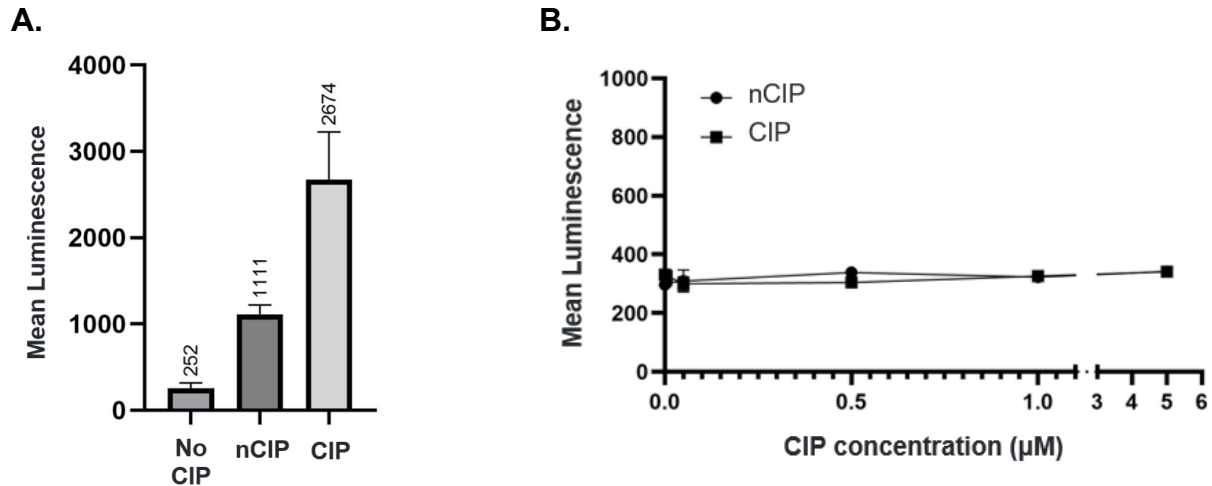
**Figure 20. Installation of the targeting domain on the cell surface using SPAAC click chemistry.** U937 monocytes were incubated with Nt-CIP-Az for 24 hours. The cells were then treated with DBCO-biotin for three hours. Targeting domain installation measured by measuring the fluorescence of a streptavidin-PE reporter molecule using flow cytometry. All controls were conducted using 1000 nM CIP/nCIP. Errors are standard deviation. \*\*\* =  $p < 0.005$

Figure 20 shows that the tumor targeting domain can be installed after the CIP has labeled CD64 on the cell surface. Treatment 1000 nM CIP with the targeting domain installed via SPAAC on the cell surface resulted in a similar mean fluorescence intensity to when the CIP was pre-clicked with the targeting domain (light blue). Labeling increased in a concentration-dependent manner, similar to when CIP was pre-clicked with the targeting domain. Notably, nCIP is still less effective than CIP when the targeting domain is installed post CD64 labeling.

Next, we wanted to investigate if we can use inverse electron demand diels-alder (IEDDA) click chemistry instead of SPAAC click chemistry to install the targeting domain. IEDDA click chemistry is more therapeutically useful as it reacts significantly faster than SPAAC. CIPs with a trans-cyclooctyne (TCO) moiety were incubated with IFN $\gamma$  activated U937 cells for 24 hours at 37 °C. The cells were then treated with an equimolar amount of biotin-tetrazine for 3 hours at 37 °C. Streptavidin-PE was added to determine the amount of biotin installed on the cell surface. A CIP-biotin molecule, where a DBCO-biotin was pre-clicked onto the azide on the peptide, was also assayed for comparison. In contrast to SPAAC, the IEDDA click strategy resulted in significantly lower fluorescence signal compared to the 'pre-clicked' compound, suggesting that IEDDA click is very ineffective (Appendix 4). We hypothesize that this is due to rapid isomerization of the TCO into an inactive form.

### **3.7 CIPs can Promote Immune Activation**

After establishing that CIPs can label CD64 effectively and specifically on the cell surface, we wanted to investigate if this labeling can promote immune cell activation. We used a reporter THP1 macrophage cell line, THP-1 NF-kB-Luc2, which is engineered to produce luciferase when the NF-kB pathway is activated. NF-kB signaling can arise from the stimulation of many activating receptors and regulates thousands of response genes encoding regulatory molecules such as cytokines, chemokines, transcription factors, and antimicrobial peptides.<sup>81</sup> Therefore, it is important for inflammatory response by innate immune cells. In this assay, luciferase production represents the extent of immune activation. Luciferase production is measured by monitoring luminescence using a microplate reader.



**Figure 21. THP1 NF- $\kappa$ B-Luc2 Macrophage Luciferase Activation Assay.** The THP1 NF- $\kappa$ B-Luc2 reporter cell line used produces luciferase when activated. Luciferase production is measured by monitoring luminescence signal using a microplate reader and correlates to the extent of macrophage activation. This assay was conducted by Dr. Mauro Castellarin. A) Macrophage activation by CIP or nCIP labeled microspheres. An effector to bead ratio of 1:5 was used. Errors are standard deviation. B) Macrophage activation by free CIP or nCIP. Errors are standard deviation.

Figure 21A shows that treatment with CIP co-incubated with a target bead increased luminescence significantly from the baseline when beads with no CIP functionalized to them were added to the macrophages. This shows that CIPs can effectively stimulate activation of the immune cell. Notably, treatment of the reporter cells with beads functionalized with noncovalent nCIP resulted in less activation, illustrating that covalency leads to an advantage in immune activation efficacy. We hypothesize that this advantage is due to covalency resulting in longer CD64 occupancy times. Kinetic proofreading refers to the idea that specificity in biochemical pathways is the result of multiple intermediate reactions. Once an immune receptor binds its ligand, a sequence of intermediate reactions need to occur before an immune response is promoted. For these reactions to occur, the receptor needs to remain bound. Ligands that have a faster rate of dissociation are less likely to induce an immune response as

the ligand will likely dissociate before the signal is completely transmitted. The idea of kinetic proofreading is reflected in this system. Covalency prevents CIPs from dissociating, ensuring that CIPs once labeled will completely promote immune activation whereas nCIPs likely often dissociate before the immune response pathway is completely activated.

Further, treatment of the reporter cell line with free CIP or nCIP, not functionalized to a bead, resulted in no activation (Figure 21B). This suggests that clustering of CD64 via binding to the target surface is needed for immune activation. This is advantageous as it reduces the risk of activating a non-specific off target immune response from CIP labeling and increases targeting specificity.

We further investigated CIPs ability to induce an immune response by monitoring CIP dependent phagocytosis of target streptavidin beads using a two-colour flow cytometry assay. IFN $\gamma$  activated U937 monocytes were pre-treated with CIP-biotin for 24 hours prior to being fluorescently dyed and co-incubated with fluorescent streptavidin-labeled beads for 1 hour at 37 °C. Fluorescence was then measured using flow cytometry. Events that were double positive for both bead fluorescence and monocyte fluorescence indicated successful phagocytosis.

Figure 22A shows the flow cytometry scatterplot when no CIP is incubated with the monocytes. Q2 represents the double positive fluorescence signal that indicates successful phagocytosis. There are few events in Q2, illustrating that very little phagocytosis occurs in the absence of CIP treatment. In contrast, when the monocytes were treated with 640 nM CIP-biotin (Figure 22B), Q2 had noticeably more events. The

histograms show visually that CIP treatment can induce significantly more phagocytosis of target beads compared to baseline.

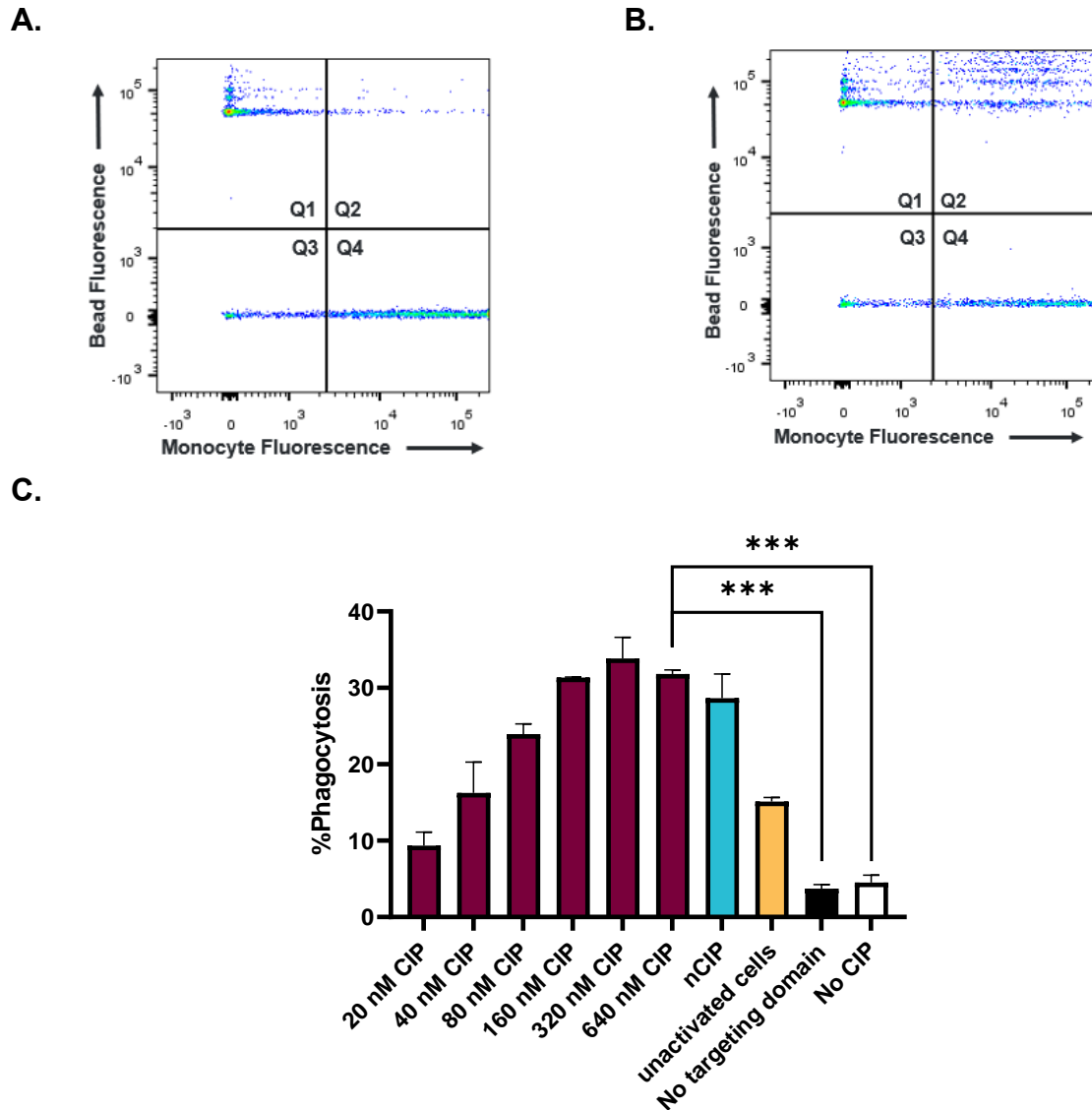


**Figure 22. Evaluation of CIP ability to induce targeted phagocytosis.** Phagocytosis of fluorescent streptavidin beads by U937 monocytes labeled with Nt-CIP-biotin was monitored using a two-colour flow cytometry assay. Successful phagocytosis was visualized as an event that is double positive for both monocyte fluorescence and bead fluorescence. A) Flow cytometry histogram showing bead fluorescence versus monocyte fluorescence with no CIP treatment. Q2 represents double positive fluorescence indicating successful phagocytosis. B) Flow cytometry histogram showing bead fluorescence versus monocyte fluorescence with 640 nM CIP treatment. Q2 represents double positive fluorescence indicating successful phagocytosis. C) calculated %phagocytosis. %phagocytosis is calculated from the histogram by comparing the double positive events (Q2) with the total monocyte fluorescence events (Q2 + Q4). All controls were conducted at 640 nM CIP/nCIP. Errors are standard deviation. \*\*\* =  $p < 0.005$

%phagocytosis is calculated from the histogram by calculating the ratio of double positive events (Q2) over total monocyte fluorescence events (Q2 + Q4) (Equation 2). %phagocytosis increases with CIP concentration and appears to plateau around 320 nM CIP-biotin (Figure 22C). This value is higher than expected given the  $K_d$  of the peptide, however it is likely that a significant fraction of CIP is inactivated over the course of the 24-hour incubation period resulting in the need for higher concentrations of CIP. Possible pathways of degradation include internalization of the CIP by the immune cells as well as the propensity of the cP33 peptide to form inactive aggregates in solution.

Notably, cells that were treated with 640 nM of CIP-Az (no biotin targeting domain) were unable to successfully phagocytose the target beads. This again suggests that CD64 clustering via binding of the target surface is needed to induce phagocytosis. Without binding of the targeting domain, CIPs cannot induce phagocytosis, illustrating that CIPs are target specific and unlikely to induce a non-specific off-target immune response. Further, when the phagocytosis assay was conducted with unactivated U937 cells that had lower surface CD64 expression, %phagocytosis decreases significantly. This suggests that the ability of CIPs to induce phagocytosis is specific to CD64 labeling.

Unexpectedly, treatment with 640 nM noncovalent analog nCIP-biotin resulted in a similar %phagocytosis as treatment with 640 nM CIP-biotin. This contrasts with previous experiments that showed that nCIP could not engage CD64 on the cell surface as effectively as CIP. However, there is a very high density of streptavidin on the surface of the bead and the bond between biotin and streptavidin is extremely high affinity. This artificially high avidity high affinity interaction could promote receptor occupancy allowing for a similar effect to that of covalency.

Changing the target could allow us to better visualize a covalent advantage. Tumour antigens bind their ligands with much lower affinity and have much lower surface expression levels. Conditions that promote ligand dissociation such as lower concentrations (sub  $K_D$ ) of CIP/nCIP and the presence of serum IgG competitor could result in a more significant covalent advantage. Notably, these conditions described are more biologically relevant.

To compare the efficacy of direct activating receptor labeling to an antibody mediated treatment, we repeated the phagocytosis assay with an analogous antibody-mediated cARM condition. The cARM used was a previously published cARM from the Rullo Lab that binds and covalently labels an anti-DNP IgG antibody and has a biotin targeting domain.<sup>61,62</sup> Treatment with the CIP induced significantly higher phagocytosis compared to the cARM treatment, suggesting that direct activating receptor labeling is more effective than an antibody-mediated treatment (Figure 23).

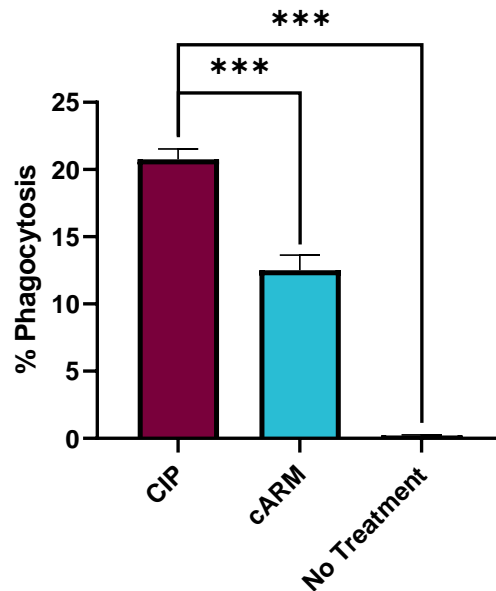


**Figure 23. Comparing the ability of CIPs and an antibody-based treatment (cARM) to induce phagocytosis using a two-colour flow cytometry assay.** Successful phagocytosis was visualized as an event that is double positive for both monocyte fluorescence and bead fluorescence. %phagocytosis is calculated from the histogram by comparing the double positive events with the total monocyte fluorescence events. The cARM treatment was an SPE7 anti-DNP antibody that was covalently functionalized with a biotin targeting domain using a small molecule cARM. Errors are standard deviation. \*\*\* =  $p < 0.005$

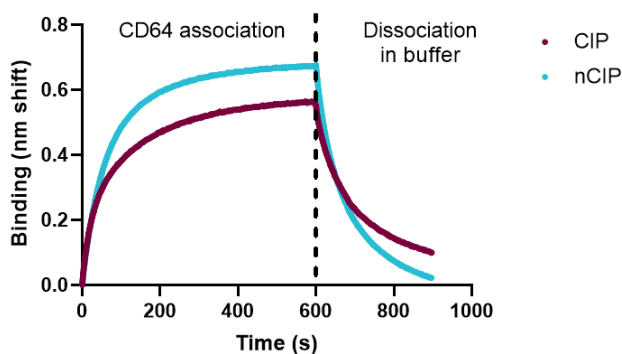
### 3.8 Future Directions: CIP-AE133 can be used to Target uPAR

While we have shown that CIP can successfully induce an immune response using a model biotin target system, we wanted to investigate whether CIP could induce an anti-tumoral immune response when targeting a biologically relevant tumor antigen. To do this, we synthesized a CIP analog that has a uPAR targeting peptide (AE133) serving as the tumor targeting domain (CIP-AE133).

After successful synthesis, we wanted to investigate if CIP-AE133 can form a ternary complex between CD64 and uPAR using bio-layer interferometry (BLI). In BLI, mass associating onto the BLI biosensor is monitored as a function of optical

wavelength shift. We tested if CIP-AE133, or its noncovalent analog (nCIP), bound to CD64 can simultaneously engage uPAR immobilized on a biosensor (Figure 24A). The streptavidin-coated biosensor was first dipped into a solution of biotinylated uPAR to load the protein onto the probe. The sensor was then dipped a solution of 500 nM CIP and 500 nM CD64. Ternary complex formation was monitored for 10 minutes by measuring the association of CD64 onto the probe. It is important to note that the concentration and times used in this assay do not allow for significant covalent labeling to occur.

**A.**



**B.**

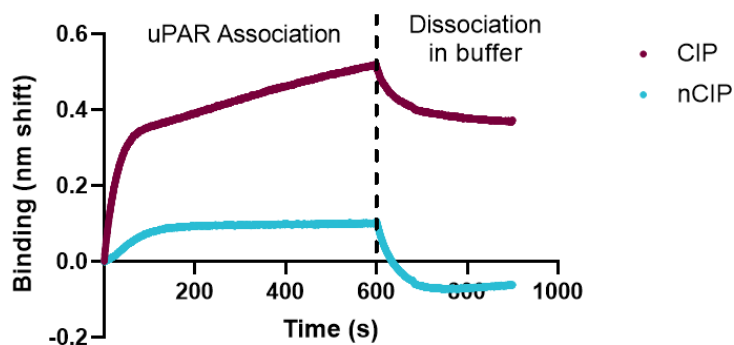


**Figure 24. Characterizing CIP-AE133 ternary complex formation using BLI.** A) BLI is used to monitor the binding of CD64 pre-equilibrated with CIP/nCIP to uPAR immobilized on a biosensor. B) BLI is used to monitor the binding of uPAR pre-equilibrated with CIP/nCIP to CD64 immobilized on a biosensor.

Both CIP and nCIP showed CD64 successfully associating onto the probe, consistent with ternary complex formation. CIP and nCIP were both able to form a ternary complex between uPAR and CD64 with equal efficacy. We then wanted to investigate if binding order affected ternary complex formation. In Figure 24B, BLI was used to monitor if CIP/nCIP pre-bound to uPAR can bind CD64 immobilized on a biosensor. CIP was again able to form a ternary complex between uPAR and CD64. However, nCIP was unable to form a ternary complex as effectively as CIP.

To determine if CIP-AE133 can induce an immune response, we repeated the previously described two-colour flow cytometry phagocytosis assay with uPAR labeled fluorescent beads (Figure 25). Treatment with 100 nM and 1000 nM CIP showed a significant increase in %phagocytosis compared to the no treatment control, illustrating that CIP-AE133 can successfully induce an immune response towards a biologically relevant tumor target. Further, treatment with 100 nM CIP induced a modest but significant enhancement in phagocytosis compared to treatment with 100 nM nCIP, consistent with a covalent functional enhancement in receptor activation. This increase in efficacy is less noticeable at higher concentrations of 1000 nM CIP/nCIP.

However, it is important to note that for this phagocytosis experiment, CIP-AE133 was only incubated with monocytes for 2 hours. Therefore, not enough time was allowed for significant covalent labeling to occur. In addition, nCIP also tightly binds CD64 due to the low  $K_D$  of cP33. LC-MS of the CIP-AE133 stock showed the presence of some excess free AE133-DBCO that could act as a competitor for uPAR binding (Appendix 5). Taken together, this illustrates that even with a low amount of covalent

labeling and unfavorable conditions, covalency can still have a great effect on efficacy as CIP outperforms nCIP.

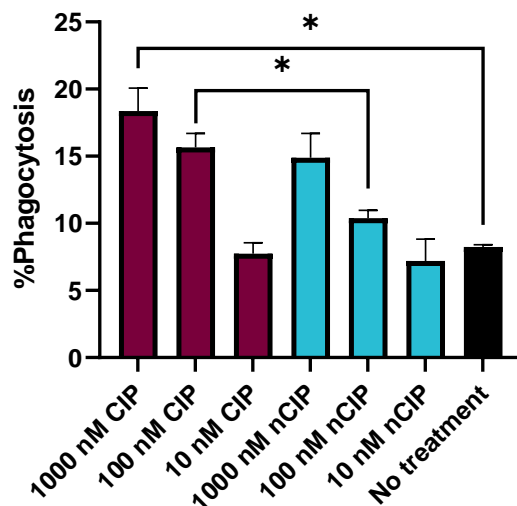


**Figure 25. Evaluating CIP-AE133 ability to induce phagocytosis of uPAR labeled targets.** CIP-AE133 can induce phagocytosis of uPAR labeled beads as illustrated using a two-colour flow cytometry phagocytosis assay. %phagocytosis is calculated from the histogram by comparing the double positive events (successful phagocytosis) with the total monocyte fluorescence events. Errors are standard deviation. \* =  $p < 0.02$

## 4. Conclusions and Future Directions

### 4.1 Conclusions

This thesis has described the design and characterization of covalent immune programmers (CIPs) that can directly label the activating receptor CD64 on the immune cell surface. The CIPs can then engage the tumor cell surface by binding specific tumor antigens using their tumor binding domain and facilitate immune cell clearance of the tumor cells. To guide future design principles, we have shown that covalent electrophile position is important to consider as changing the position of the SuFEx within the CIP leads to different labeling efficacy and aqueous stability. We have shown that CIPs can label CD64 both in solution and on the surface of the immune cell specifically and

irreversibly. Notably, covalent CIP was observed to engage CD64 more effectively compared to a non-covalent analog. CIP labeling can facilitate macrophage activation and induce target phagocytosis using a biotin-streptavidin bead model system. THP-1 NFkB-Luc2 engineered reporter macrophage activation assays demonstrated that covalency can increase immune cell activation efficacy. Comparison in phagocytosis assays suggests that direct activating receptor engagement using CIPs can outperform antibody-mediated treatments.

A CIP analog that can engage the tumor marker uPAR using AE133 peptide as its tumor targeting domain was developed (CIP-AE133). Preliminary characterization of CIP-AE133 shows that it can successfully bridge CD64 and uPAR in BLI binding assays. Further, CIP-AE133 can induce phagocytosis of uPAR labeled target beads. There is some evidence that CIP-AE133 can outperform its non-covalent analog. Taken together, these insights establish CIPs as a promising new immunotherapeutic platform and its use of direct activating receptor labeling can improve upon current strategies in development.

## **4.2 Future Directions**

Preliminary work has been done to develop CIPs that can target biologically relevant tumor antigen uPAR, however this system can be further optimized. First, CIP-AE133 purity should be improved by adding an HPLC purification step after AE133 installation. Without the excess unclicked AE133 peptide acting as a competitor, we can better determine CIP immune programming efficacy. Determining optimal CIP-AE133 labeling time can also help increase CIP efficacy in phagocytosis assays. Development

of a Western blot approach to visualize the extent of covalently labeled CD64 on the immune cell surface could help further validate the conclusions in this thesis.

Development of CIPs with other tumor targeting domains can further illustrate the versatility of the CIP platform. Potential tumor targets to investigate include glutamate urea lysine to target prostate-specific membrane antigen in the treatment of prostate cancer or a HER2 binding peptide (sequence: Q-D-V-N-T-A-V-A-W) in the treatment of breast cancer.<sup>93</sup>

As well, investigation into CIP internalization and labeled receptor recycling can help further understanding of the CIP-immune cell interaction. Understanding how long CIP remains on the surface of the cell can aid in determining treatment dosage and incubation times. pHrodo Red is a pH sensitive dye that is non-fluorescent on the cell surface but is highly fluorescent when internalized in the acidic lysosome environment.<sup>92</sup> Conjugating this dye to CIP could allow us to monitor CIP internalization rates using flow cytometry. Further, to determine if intact CIP can be recycled to cell surface, we can use an immunofluorescence quenching assay. Recycling of Alexa Fluor 488 tagged CIP can be visualized by fluorescence quenching using an anti-Alex Fluor 488 antibody after labeling. Ultimately, these pursuits can help in translating CIP function to an *in vivo* model.

## 5. References

1. Sung, H.; Ferlay, J.; Siegel, R.; Laversanne, M.; Soerjomataram, I.; Jemal, A.; and Bray, F. Global Cancer Statistics 2020: GLOBOCAN Estimates of Incidence and Mortality Worldwide for 36 Cancers in 185 Countries. *CA: Cancer J. Clin.* **2021**, *71*, 209-249, DOI: 10.3322/caac.21660
2. Bray, F.; Laversanne, M.; Weiderpass, E.; and Soerjomataram, I. The Ever-Increasing Importance of Cancer as a Leading Cause of Premature Death Worldwide. *Cancer.* **2021**, *127*, 3029-3030, DOI: 10.1002/cncr.33587
3. Arruebo, M.; Vilaboa, N.; Saez-Gutierrez, B.; et al. Assessment of the Evolution of Cancer Treatment Therapies. *Cancers.* **2011**, *3*, 3279-330.
4. Moses, M.A.; Brem, H.; and Langer, R. Advancing the Field of Drug Delivery: Taking Aim at a Cancer. *Cancer Cell.* **2003**, *4*, 337-341.
5. Dagogo-Jack, I.; and Shaw, A.T. Tumour Heterogeneity and Resistance to Cancer Therapies. *Nat Rev Clin Oncol.* **2018**, *15*, 81-94. DOI: 10.1038/nrclinonc.2017.166.
6. Neves, H.; and Kwok, H.F. Recent advances in the field of anti-cancer immunotherapy. *BBA Clin.* **2018**, *3*, 280-288.
7. June, C.H.; O'Connor, R.S.; Kawalekar, O.U.; Ghassemi, S. and Milone, M.C. CAR T Cell Immunotherapy for Human Cancer. *Science.* **2018**, *359*, 1361-1365.
8. Mahoney, K.M.; Rennert, P.D.; and Freeman, G.J. Combination Cancer Immunotherapy and New Immunomodulatory Targets. *Nat Rev Drug Disc.* **2015**, *14*, 561-584.
9. Rosenberg, S.A.; Lotze, M.T.; Yang, J.C.; Aebersold, P.M.; Linehan, W.M.; Seipp, C.A. et al. Experience with the use of High-Dose Interleukin-2 in the Treatment of 652 Cancer Patients. *Ann Surg.* **1989**, *210*, 474-484.
10. Grimm, E.A.; Mazumder, A.; Zhang, H.Z.; and Rosenberg, S.A. Lymphokine-activated Killer Cell Phenomenon, Lysis of Natural Killer-Resistant Fresh Solid Tumour Cells by Interleukin 2-Activated Autologous Human Peripheral Blood Lymphocytes. *J. Exp. Med.* **1982**, *155*, 1823-1841.
11. Yokosuka, T.; Takamatsu, M.; Kobayashi-Imanishi, W.; Hashimoto-Tane, A.; Azuma, M.; and Saito, T. Programmed Cell Death 1 Forms Negative Costimulatory Microclusters that Directly Inhibit T Cell Receptor Signalling by Recruiting Phosphatase SHP2. *J. Exp. Med.* **2012**, *209*, 1201-1217.
12. Grzywnowicz, M.; Zaleska, J.; Mertens, D.; Tomczak, W.; Wlasiuk P.; Kosior, K.; Piechnik, A.; Bojarska-Junak, A.; Dmoszynska, A.; and Giannopoulos, K. Programmed Death-1 and its Ligand are Novel Immunotolerant Molecules Expressed on Leukemic B Cells in Chronic Lymphocytic Leukemia. *PLoS ONE.* **2012**, *7*, e35178.
13. Topalian, S.L.; Hodi, F.S.; Brahmer, J.R.; Gettinger, S.N.; Smith, D.C.; McDermott, D.F.; Powderly, J.D.; Carvajal, R.D.; Sosman, J.A.; Atkins, M.B.; Leming, P.D.; Spigel, D.R.; Antonia, S.J.; Horn, L.; Drake, C.G.; Pardoll, D.M.; Chen, L.; Sharfman, W.H.; Anders, R.A.; Taube, J.M.; McMiller, T.L.; Xu, H.; Korman, A.J.; Jure-Kunkel, M.; Agrawal, S.; McDonald, D.; Kollia, G.D.; Gupta, A.; Wigginton, J.M.; and Sznol, M. Safety, Activity and Immune Correlates of anti-PD-1 Antibody in Cancer. *New England Journal of Medicine.* **366**, 2443-2454.
14. Vogel, C.L. et al. Efficacy and Safety of Trastuzumab as a Single Agent in the First-Line Treatment of HER-2 Overexpressing Metastatic Breast Cancer. *J Clin. Oncol.* **2002**, *20*, 719-726.

15. McLaughlin, P. et al. Rituximab Chimeric Anti-CD20 Monoclonal Antibody Therapy for Relapsed Indolent Lymphoma: Half of Patients Respond to a Four-dose Treatment Program. *J. Clin. Oncol.* **1998**, *16*, 2825-2833.
16. Tan, S.; Li, D.; and Zhu, X. Cancer Immunotherapy: Pros, Cons, and Beyond. *Biomed. Pharmacother.* **2020**, *124*, 109821.
17. Wei, G.; Wang, J.; Huang, H.; and Zhao, Y. Novel immunotherapies for adult patients with B-lineage acute lymphoblastic leukemia. *J. Hematol. Oncol.* **2017**, *10*, 150.
18. Marei, H.E.; Althani, A.; Caceci, T.; Arriga, R.; Sconocchia, T.; Ottaviani, A.; Lanzilli, G.; Roselli, M.; Caratelli, S.; Cenciarelli, C.; and Sconocchia, G. Recent Perspective on CAR and Fcγ-CD3 T cell Immunotherapy for Cancers: Preclinical Evidence Versus Clinical Outcomes. *Biochem. Pharmacol.* **2019**, *166*, 335-346.
19. Leach, D.R.; Krummel, M.F.; and Allison, J.P. Enhancement of Antitumor Immunity by CTLA-4 Blockade. *Science.* **1996**, *271*, 1734-1736.
20. Ghorashian, S. et al. Enhanced CAR T cell Expansion and Prolonged Persistence in Pediatric Patients with ALL Treated with a Low-affinity CD19 CAR. *Nat. Med.* **2019**, *25*, 1408-1414.
21. Dunn, G.P.; Old, L.J.; and Schreiner, R.D. The Immunobiology of Cancer Immunosurveillance and Immunoediting. *Immunity.* **2004**, *21*, 137-148.
22. Prendergast, G.C. Immune Escape as a Fundamental Trait of Cancer: Focus on IDO. *Oncogene.* **2008**, *27*, 3889-3900.
23. Hegde, P.S.; Karanikas, V.; and Evers, S. The Where, the When and the How of Immune Monitoring for Cancer Immunotherapies in the Era of Checkpoint Inhibition. *Clin Cancer Res.* **2016**, *22*. DOI: 10.1158/1078-0432.CCR-15-1507
24. Bruni, D.; Angell, H.K.; and Galon, J. The Immune Contexture and Immunoscore in Cancer Prognosis and Therapeutic Efficacy. *Nat. Rev. Cancer.* **2020**, *20*, 662-680.
25. Liu, Y.T.; and Sun, Z.J. Turning Cold Tumours into Hot Tumours by Improving T-Cell Infiltration. *Theranostics.* **2021**, *11*, 5365.
26. Chaplin, D. Overview of the Immune Response. *J. Allergy Clin. Immunol.* **2010**, *125*, S3-S23.
27. Smith, N.C.; Rise, M.; and Christian, S.L. A Comparison of the Innate and Adaptive Immune Systems in Cartilaginous Fish, Ray-Finned Fish, and Lobe-Finned Fish. *Front. Immunol.* **2019**, *10*, DOI: 10.3389/fimmu.2019.02292
28. Akkin, S.; Varan, G.; and Bilensoy, E. A Review on Cancer Immunotherapy and Applications of Nanotechnology to Chemotherapy of Different Cancers. *Molecules.* **2021**, *26*, DOI:10.3390/MOLECULES26113382
29. Luckheeram, R.V.; Zhou, R.; Verma, A.D.; and Xia, B. CD4(+)T cells: Differentiation and Functions. *Clin Dev Immunol.* **2012**, DOI: 10.1155/2012/925135
30. Robert, J. Comparative Study of Tumorigenesis and Tumour Immunity in Invertebrates and Nonmammalian Vertebrates. *Dev. Comp. Immunol.* **2010**, *34*, 915-925.
31. Franken, L.; Schiwon, M.; and Kurts, C. Macrophages: sentinels and regulators of the immune system. *Cell Microbiol.* **2016**, *18*, 475-487.
32. Duan, Z.; and Luo, Y. Targeting Macrophages in Cancer Immunotherapy. *Signal Transduct. Target Ther.* **2021**, *6*, 127.
33. Karlmark, K.R.; Tacke, F.; and Dunay, I.R. Monocytes in Health and Disease – Minireview. *Eur. J. Microbiol. Immunol.* **2012**, *2*, 192.
34. O'Sullivan, T. et al. Cancer Immunoediting by the Innate Immune System in the Absence of Adaptive Immunity. *J. Exp. Med.* **2012**, *209*, 1869-1882.

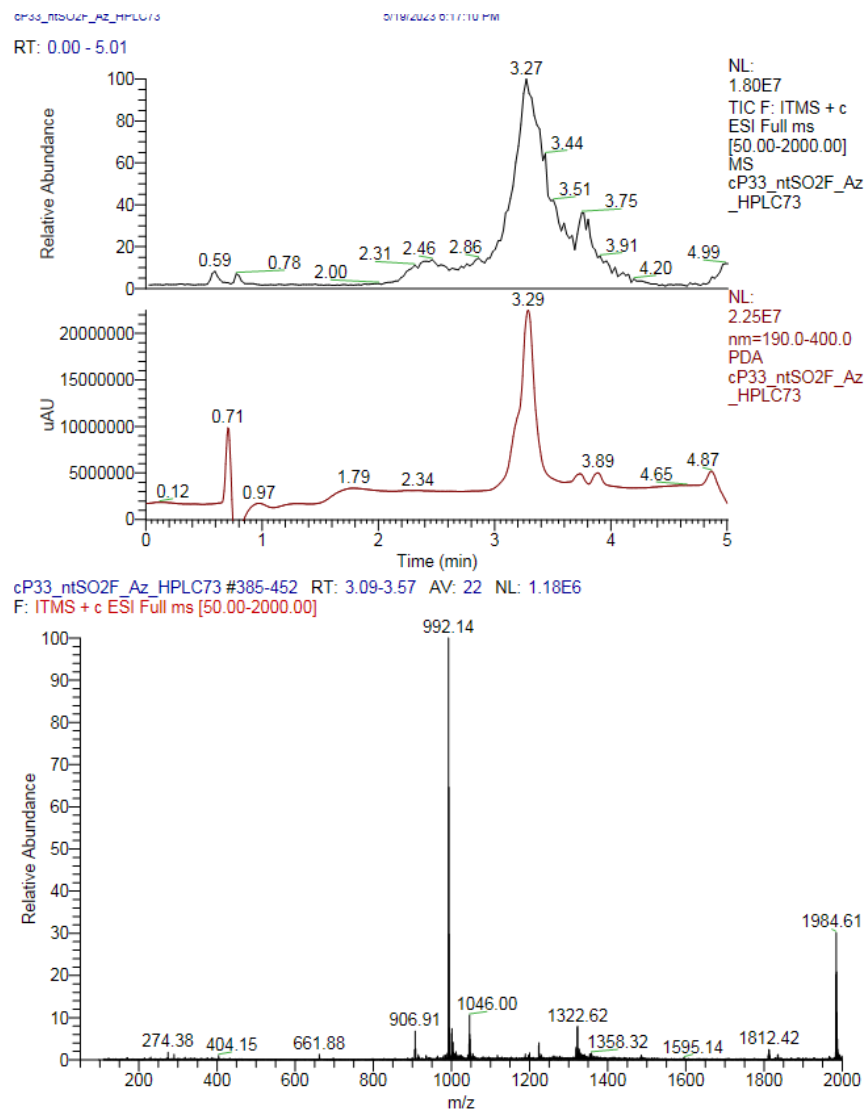
35. Mills C.D.; Shearer, J.; Evans, R.; and Caldwell, M.D. Macrophage Arginine Metabolism and the Inhibition or Stimulation of Cancer. *J. Immunol.* **1992**, *149*, 2709-2714.
36. Bonnardel, J.; and Guilliams, M. Developmental Control of Macrophage Function. *Curr. Opin. Immunol.* **2018**, *50*, 64-74.
37. Epelman, S.; Lavine, K.J.; and Randolph, G.J. Origin and Functions of Tissue Macrophages. *Immunity.* **2014**, *41*, 21-35.
38. Lavin, Y.; Mortha, A.; Rahman, A.; and Merad, M. Regulation of Macrophage Development and Function in Peripheral Tissues. *Nat. Rev. Immunol.* **2015**, *15*, 731-744.
39. Ginhoux, F.; and Guilliams, M. Tissue-resident Macrophage Ontogeny and Homeostasis. *Immunity.* **2016**, *44*, 439-449.
40. Gruganm K.D.; McCable, F.L.; Kinder, M.; Greenplate, A.R.; Harman, B.C.; Ekert, J.E.; van Rooijen, N.; Anferon, G.M.; Nemeth, J.A.; Strohl, W.R.; et al. Tumour-associated macrophages promote invasion while retaining Fc dependent anti-tumour function. *J. Immunol.* **2012**, *189* (11), 5457-5466.
41. DeNardo, D.G.; and Ruffell, B. Macrophages as Regulators of Tumour Immunity and Immunotherapy. *Nat Rev Immunol.* **2019**, *19*, 369-382.
42. Ran, D.; and Montgomery, K.E.; Macrophage-mediated Lymphangiogenesis: The Emerging Role of Macrophages as Lymphatic Endothelial Progenitors. *Cancers.* **2012**, *4*, 618-657.
43. Rao, S.; et al. Obligatory Participation of Macrophages in an Angiopoietin 2 Mediated Cell Death Switch. *Development.* **2007**, *134*, 4449-4458.
44. Stefater, J.A.; et al. Regulation of Angiogenesis by a Non-canonical Wnt Flt1 Pathway in Myeloid Cells. *Nature.* **2011**, *474*, 511-515.
45. Spiric, Z.; Eri, Z.; and Eric, M. Significance of Vascular Endothelial Growth Factor (VEGF) C and VEGF-D in the Progression of Cutaneous Melanoma. *Int. J. Surg.* **2015**, *23*, 629-637.
46. Jeong, H. et al. Tumour-associated Macrophages Enhance Tumour Hypoxia and Aerobic Glycolysis. *Cancer Res.* **2019**, *79*, 795-806.
47. Feng, J. et al. Emerging Roles and the Regulation of Aerobic Glycolysis in Hepatocellular Carcinoma. *J. Exp. Clin. Cancer. Res.* **2020**, *39*, 126.
48. Srinivasan, S. et al. Hypoxia-induced Expression of Phosducin-like 3 Regulates Expression of VEGFR-2 and Promotes Angiogenesis. *Angiogenesis.* **2015**, *18*, 449-462.
49. Wynn, T.A.; Chawla, A.; and Pollard, J.W. Macrophage Biology in Development, Homeostasis, and Disease. *Nature.* **2013**, *496*, 445-455.
50. Wang, W.; et al. miR-100 Maintains Phenotype of Tumour Associated Macrophages by Targeting mTOR to Promote Tumour Metastasis via Stat5a/IL-1ra Pathway in Mouse and Breast Cancer. *Oncogenesis.* **2018**, *7*, 97.
51. Li, X.; et al. Harnessing Tumour-Associated Macrophages as Aids for Cancer Immunotherapy. *Mol Cancer.* **2019**, *18*, 177.
52. Petty, A.J.; Owen, D.H.; Yang, Y.; and Huang, X. Targeting Tumour-Associated Macrophages in Cancer Immunotherapy. *Cancers.* **2021**, *13*, 5318.
53. Singh, M.; Khong, H.; Dai, Z.; Huang, X.F.; Wargo, J.A.; Cooper, Z.A.; Vasilakos, J.P.; Hwu, P.; and Overwijk, W.W. Effective Innate and Adaptive Antimelanoma Immunity through Localized TLR7/8 Activation. *J. Immunol.* **2014**, *193*, 4722-4731.
54. Menzies, S.; Mc Menamin, M.; and Barry, R. Lentigo maligna successfully treated with combination therapy of topical tazarotene and imiquimod. *Clin Exp Dermatol.* **2017**, *42*(4), 478-470.

55. Vonderheide, R.H.; Flaherty, K.T.; Khalil, M.; Stumacher, M.S.; Bajor, D.L.; Hutnick, N.A.; et al. Clinical activity and immune modulation in cancer patients treated with CP-870,893, a novel CD40 agonist monoclonal antibody. *J. Clin. Oncol.* **2007**, *25*(7), 876-883.
56. Rodell, C.B.; Arlauckas, S.P.; Cuccarese, M.F.; Garris, C.S.; Li, R.; Ahmed, M.S.; et al. TLR7/8-agonist-loaded nanoparticles promote the polarization of tumour-associated macrophages to enhance cancer immunotherapy. *Nat Biomed Eng.* **2018**, *2*(8), 578-588.
57. Liu, M.; O'Connor, R.S.; Trefely, S.; Graham, K.; Snyder, N.W.; and Beatty, G.L. Metabolic rewiring of macrophages by CpG potentiates clearance of cancer cells and overcomes tumour-expressed CD47-mediated 'don't eat me signal'. *Nat Immunol.* **2019**, *20*(2), 265-275.
58. Dunn, G.P.; Koebel, C.M.; and Schreiber, R.D. Interferons, immunity and cancer immunoediting. *Nat Rev Immunol.* **2006**, *6*(11), 836-848.
59. Salomon, R.; and Dahan, R. Next generation CD40 agonistic antibodies for cancer immunotherapy. *Front. Immunol.* **2022**, *13*,
60. Liu, M.; Luo, F.; Ding, C.; Albeituni, S.; Hu, X.; Ma, Y.; Cai, Y.; McNally, L.; Sanders, M.; Jain, D.; Goetz, K.; Bousamra, M.; Zhang, H.; Higashi, R.M.; Lane, A.N.; Fan, T.; and Yan, J. Dectin-1 activation by a natural product  $\beta$ -glucan converts immunosuppressive macrophages into an M1-like phenotype. *J Immunol.* **2015**, *195*(10), 5055-5065.
61. Kaneda, M.M.; Messer, K.S.; Ralainirina, N.; Li, H.; Leem, C.J.; Gorjestani, S.; Woo, G.; Nguyen, A.V.; Figueiredo, C.C.; Foubert, P. et al. PI3K $\gamma$  is a molecular switch that controls immune suppression. *Nature.* **2016**, *539*, 437-442.
62. Petty, A.J.; Li, A.; Wang, X.; Dai, R.; Heyman, B.; Hsu, D.; Huang, X.; Yang, Y. Hedgehog Signalling Promotes Tumour-associated Macrophage Polarization to Suppress Intratumoral CD8+ T cell Recruitment. *J Clin. Investig.* **2019**, *129*, 5151-5162.
63. Zhang, F.; Parayath, N.N.; Ene, C.I.; Stephan, S.B.; Koehne, A.L.; Coon, M.E.; Holland, E.C.; and Stephan M.T. Genetic Programming of Macrophages to Perform Anti-Tumour Functions Using Targeted mRNA Nanocarriers. *Nat Commun.* **2019**, *10*, 3974.
64. Gutmann, M.; Bechold, J.; Seibel, J.; Meinel, L.; and Luhmann, T. Metabolic Glycoengineering of Cell-derived Matrices and Cell Surfaces: A Combination of Key Principles and Step-by-Step Procedures. *ACS Biomater. Sci. Eng.* **2019**, *5*, 215-233.
65. Wang, H.; Wang, R.; Cai, K.; He, H.; Liu, Y.; Yen, J.; Wang, Z.; Xu, M.; Sun, Y.; Zhou, X.; Yin, Q.; Tang, L.; Dobrucki, I.T.; Dobrucki, L.W.; Chaney, E.J.; Boppart, S.A.; Fan, T.M.; Lezmi, S.; Chen, X.; Yin, L.; and Cheng, J. Selective in vivo metabolic cell-labelling-mediated cancer targeting. *Nat Chem Biol.* **2017**, *13*, 415-424.
66. Sugimoto, S.; and Iwasaki, Y. Surface Modification of Macrophages with Nucleic Acid Aptamers for Enhancing the Immune Response against Tumour Cells. *Bioconjugate Chem.* **2018**, *29*, 4160-4167.
67. Sterner, R.C.; and Sterner R.M. CAR-T cell Therapy: Current Limitations and Potential Strategies. *Blood Cancer Journal.* **2021**, *11*, 69.
68. Klichinsky, M.; et al. Human Chimeric Antigen Receptor Macrophages for Cancer Immunotherapy. *Nature Biotechnology.* **2020**, *38*, 947-953.
69. Lu, R. M.; Hwang, Y. C.; Liu, I. J.; Lee, C. C.; Tsai, H. Z.; Li, H. J.; Wu, H. C. Development of Therapeutic Antibodies for the Treatment of Diseases. *J. Biomed. Sci.* **2020**, *27*, 1–30.

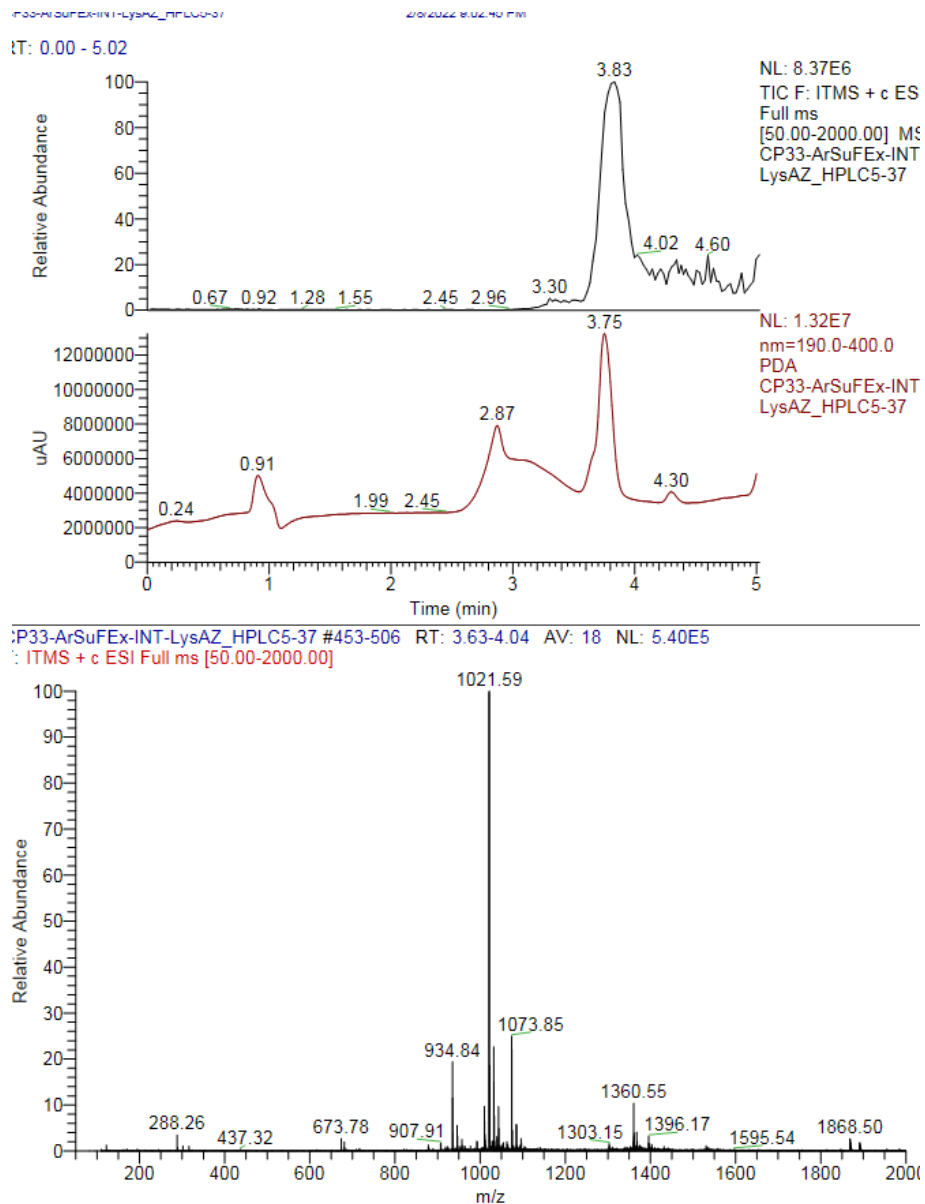
70. Dekkers, G.; Bentlage, A. E. H.; Stegmann, T. C.; Howie, H. L.; Lissenberg-Thunnissen, S.; Zimring, J.; Rispens, T.; Vidarsson, G. MAbs Affinity of Human IgG Subclasses to Mouse Fc Gamma Receptors. *MAbs*. **2017**. DOI: 10.1080/19420862.2017.1323159
71. De Chames, P.; Van Regenmortel, M.; Weiss, E.; Baty, D. Therapeutic Antibodies: Successes, Limitations and Hopes for the Future. *Br. J. Pharmacol.* **2009**, *157*, 220.
72. Murelli, R.P.; Zhang, A.X.; Michel, J.; Jorgensen, W.L.; and Spiegel, D.A. Chemical Control over Immune Recognition: A Class of Antibody-Recruiting Small Molecules That Target Prostate Cancer. *J Am Chem Soc.* **2009**, *131*, 17090-17092.
73. Lake, B.; Serniuck, N.; Kapcan, E.; Wang, A.; and Rullo, A.F. Covalent Immune Recruiters: Tools to Gain Chemical Control Over Immune Recognition. *ACS Chem. Biol.* **2020**, *15*, 1089-1095.
74. Kapcan, E.; Lake, B.; Yang, Z.; Zhang, A.; Miller, M.S.; and Rullo, A.F. Covalent Stabilization of Antibody Recruitment Enhances Immune Recognition of Cancer Targets. *Biochemistry*. **2021**, *60*, 1447-1458.
75. Nimmerjahn, F.; Ravetch, J.V.; Fcγ receptors: old friends and new family members. *Immunity*. **2016**, *24*, 19-28.
76. Bonetto, S.; Spadola, L.; Buchanan, A.G.; Jermutus, L.; Lund, J. Identification of cyclic peptides able to mimic the functional epitope of IgG1-Fc for human FcγRI. *FASEB J.* **2009**, *23*, 575-585.
77. Dong, J.; Krasnova, L.; Finn M.G.; Sharpless, K.B. Sulfur(VI) fluoride exchange (SuFEx): another good reaction for click chemistry. *Angew. Chemie Int Ed.* **2014**, *53*(36), 9430-9448.
78. Narayanan, A.; Jones, L.H. Sulfonyl fluorides as privileged warheads in chemical biology. *Chemical Science*. **2015**, *6*(5), 2650.
79. Martin-Gago, P.D.P.; Olsen, P.D.C.A. Arylfluorosulfate-based electrophiles for covalent protein labeling: a new addition to the arsenal. *Angew Chem Int Ed Engl.* **2019**, *58*(4), 957.
80. Mazar, A.P.; Ahn, R.W.; and O'Halloran, T.V. Development of novel therapeutics targeting the urokinase plasminogen activator receptor (uPAR) and their translation toward the clinic. *Curr Pharm Des.* **2011**. *17*(19), 1970-1978.
81. Elias, V.; Scully, M.F.; and Kakkar, V.V. Plasminogen activation initiated by single-chain urokinase-type plasminogen activator. Potentiation by U937 monocytes. *J. Biol. Chem.* **1989**. *264*(4). 2185-2188.
82. Zhai, B.T.; Tian, H.; Sun, J.; Zou, J.B.; Zhang, X.F.; Cheng, J.X.; Shi, Y.J.; Fan, Y.; and Guo, D.Y. Urokinase-type plasminogen activator receptor (uPAR) as a therapeutic target in cancer. *J. Trans. Med.* **2022**. *20*. 135.
83. Stephens, R.W.; Pollanen, J.; Tapiovaara, H.; Leung, K.C.; Sim, P.S.; Salonem, E.M.; Ronne, E.; Behrendt, N.; Dano, K.; Vaheri, A. Activation of pro-urokinase and plasminogen on human sarcoma cells: a proteolytic system with surface-bound reactants. *J Cell Biol.* **1989**. *108*(5). 1987-1995.
84. Yamamoto, M.; Sawaya, R.; Mohanam, S.; Rao, V.H.; Bruner, J.M.; Nicolson, G.L.; Rao, J.S. Expression and localization of urokinase-type plasminogen activator receptor in human gliomas. *Cancer Res.* **1994**, *54*(18), 5016-5020.
85. Boonstra, M.C.; Verbeek, F.P.; Mazar, A.P.; Prevo, H.A.; Kuppen, P.J.; van de Velde, C.J.; Vahrmeijer, A.L.; Sier, C.F. Expression of uPAR in tumour-associated stromal cells is associated with colorectal cancer patient prognosis: a TMA study. *BMC Cancer.* **2014**, *14*(269).

86. Ploug, M.; Ostergaard, S.; Gardsvoll, H.; Kovalski, K.; Holst-Hansen, C.; Holm, A.; Ossowski, L.; and Dano, K. Peptide-derived antagonists of the urokinase receptor. Affinity maturation by combinatorial chemistry, identification of functional epitopes, and inhibitory effect on cancer cell intravasation. *Biochemistry*. **2001**, 40(40). 12157-12168.
87. McEnaney, P.J.; Fitzgerald, K.J.; Zhang, A.X.; Douglass, E.F.; Shan, W.; Balog, A.; Kolesnikova, M.D.; and Spielgel, D.A. Chemically synthesized molecules with the targeting and effector functions of antibodies. *J Am Chem Soc*. **2014**, 136(52), 18034-18043.
88. Turner, R. Monocyte Covalent Immune Recruiters: Tools to Modulate Synthetic Immune Recognition. Master's Thesis, McMaster University, Hamilton, Canada, 2022.
89. Neumann, K.; Farnung, J.; Baldauf, S.; and Bode, J.W. Prevention of aspartimide formation during peptide synthesis using cyanosulfurylides as carboxylic acid-protecting groups. *Nat Comm*. **2020**, 11(982).
90. Subiros-Funosas, R.; El-Faham, A.; and Albericio, F. Aspartimide formation in peptide chemistry: occurrence, prevention strategies and the role of N-hydroxylamines. *Tetrahedron*. **2011**, 67(45), 8595-8606.
91. Behrendt, R.; Huber, S.; and White, P. Preventing aspartimide formation in Fmoc SPPS of Asp-Gly containing peptides-practical aspects of new trialkylcarbinol based protected groups. *J. Pep. Sci*. **2016**, 22(2), 92-97.
92. Lindner, B.; Burkard, T.; and Schuler, M. Phagocytosis assays with different pH-sensitive fluorescent particles and various readouts. *Biotechniques*. **2020**, 68(5)
93. Verdoliva, V.; Digilio, G.; Miletto, I.; Saviano, M.; and De Luca, S. Fluorescence studies: A9 peptide, functionalized with a fluorogenic probe, interacts with its receptor model HER2-DIVMP. *Acs Med Chem Lett*. **2022**, 13(5), 807-811.

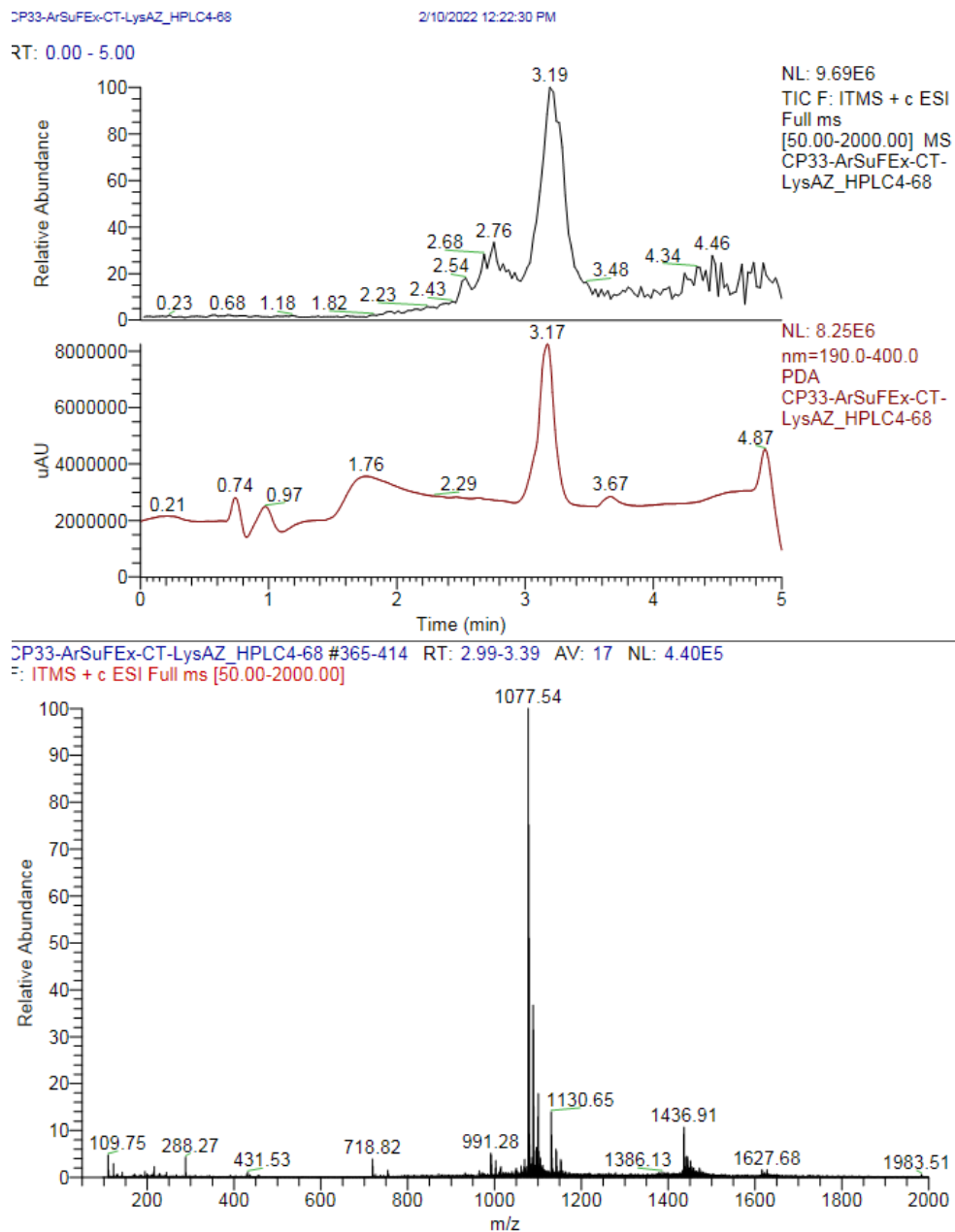
## 6. Appendix



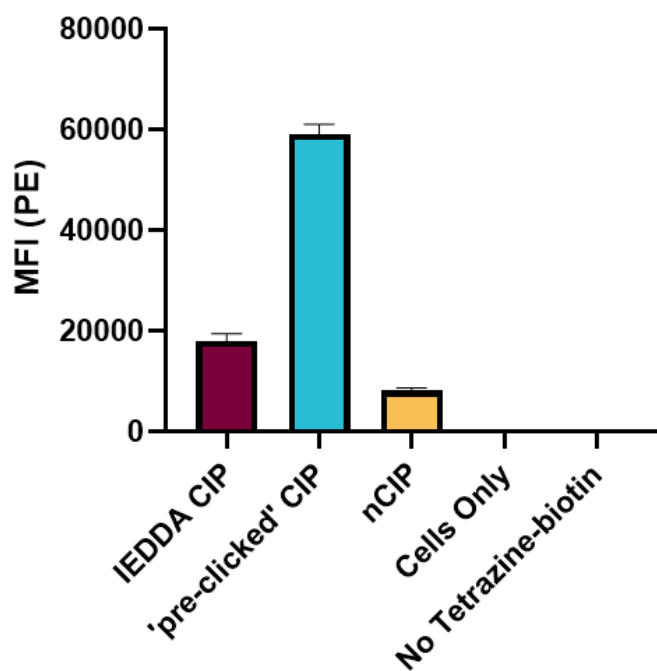
**Appendix 1. LC-MS of purified Nt-CIP-Az.** The molecular mass of Nt-CIP-Az is 1983 g/mol. The product peak eluted at 3.29 minutes. The expected  $z=1$  mass peak is seen at 1984 m/z. The expected  $z=2$  mass peak is seen at 992 m/z.



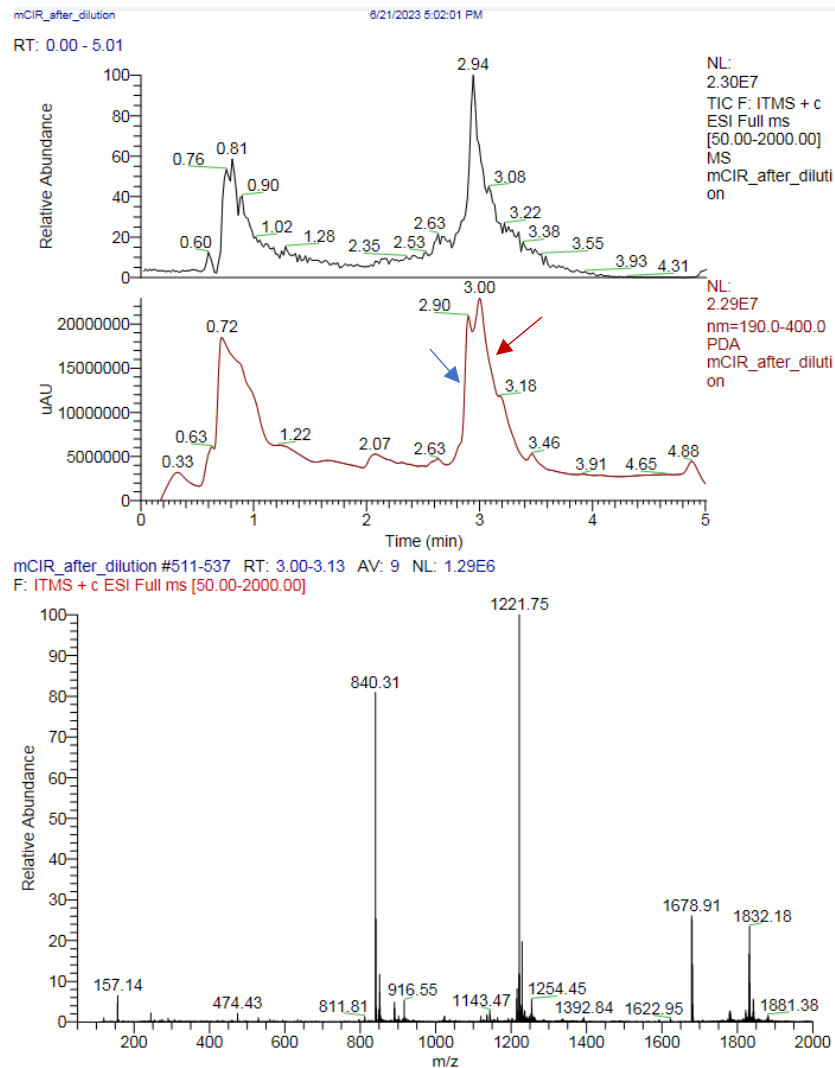
**Appendix 2. LC-MS of purified Int-CIP-Az.** The molecular mass of Nt-CIP-Az is 2040 g/mol. The product peak eluted at 3.75 minutes. The expected  $z=2$  mass peak is seen at 1021 m/z.



**Appendix 3. LC-MS of purified Ct-CIP-Az.** The molecular mass of Nt-CIP-Az is 2154 g/mol. The product peak eluted at 3.17 minutes. The expected  $z=2$  mass peak is seen at 1077 m/z.



**Appendix 4. Determination of IEDDA click strategy labeling efficacy.** U937 monocytes were labelled with CIP-TCO for 24 hours prior to addition of tetrazine-biotin. After two hours, streptavidin-PE was added to determine the amount of biotin labelled on the cell surface. The cell surface click strategy resulted in much lower labelling compared to 'pre-clicked' CIP where biotin was pre-clicked onto the CIP via SPAAC click chemistry.



**Appendix 5. LC-MS of CIP-AE133.** The molecular mass of CIP-AE133 is 3662 g/mol. The product peak eluted at 3.00 minutes (red arrow). The expected  $z=2$  mass peak for CIP-AE133 is seen at 1832 m/z. The expected  $z=2$  mass peak for CIP-AE133 is seen at 1221 m/z. The molecular mass of free AE133-DBCO is 1678 g/mol. The product peak eluted at 2.90 minutes (blue arrow). The expected  $z=1$  mass peak for AE133-DBCO is seen at 1678 m/z. The expected  $z=2$  mass peak for AE133-DBCO is seen at 840 m/z.